Pressure and temperature dependence of hydrophobic hydration: Volumetric, compressibility, and thermodynamic signatures

Maria Sabaye Moghaddam and Hue Sun Chan[a)]
Department of Biochemistry and Department of Medical Genetics and Microbiology, Faculty of Medicine, University of Toronto, Toronto, Ontario M5S 1A8, Canada

(Received 18 December 2006; accepted 16 January 2007; published online 20 March 2007)

The combined effect of pressure and temperature on hydrophobic hydration of a nonpolar methanelike solute is investigated by extensive simulations in the TIP4P model of water. Using test-particle insertion techniques, free energies of hydration under a range of pressures from 1 to 3000 atm are computed at eight temperatures ranging from 278.15 to 368.15 K. Corresponding enthalpy, entropy, and heat capacity accompanying the hydration process are estimated from the temperature dependence of the free energies. Partial molar and excess volumes calculated using pressure derivatives of the simulated free energies are consistent with those determined by direct volume simulations; but direct volume determination offers more reliable estimates for compressibility. At 298.15 K, partial molar and excess isothermal compressibilities of methane are negative at 1 atm. Partial molar and excess adiabatic (isentropic) compressibilities are estimated to be also negative under the same conditions. But partial molar and excess isothermal compressibilities are positive at high pressures, with a crossover from negative to positive compressibility at ~100–1000 atm. This trend is consistent with experiments on aliphatic amino acids and pressure-unfolded states of proteins. For the range of pressures simulated, hydration heat capacity exhibits little pressure dependence, also in apparent agreement with experiment. When pressure is raised at constant room temperature, hydration free energy increases while its entropic component remains essentially constant. Thus, the increasing unfavorability of hydration under raised pressure is seen as largely an enthalpic effect. Ramifications of the findings of the authors for biopolymer conformational transitions are discussed. © *2007 American Institute of Physics*.
[DOI: 10.1063/1.2539179]

I. INTRODUCTION

Pressure and volumetric studies have long provided fundamental as well as practical information on chemical reactions, solvation, and polymer conformational properties. As far as biomolecular processes are concerned,[1,2] since as early[3] as 1914, high pressure has been used as a probe for protein denaturation.[4] In conjunction with calorimetry,[5] compressibility measurements,[6–8] NMR,[9,10] and other experimental techniques, biophysical studies of pressure effects have been applied to investigate the emergence of partially structured intermediates upon protein unfolding,[11] formation of amyloid fibrils and dissociation of aggregated proteins,[5,12,13] stability of folded states in confined volumes,[14] effects of protein denaturants and stabilizers,[15] and folding transition states,[10]—in short, changes in hydration and packing[9] that accompany conformational transitions in general.[16,17] Volumetric considerations constitute a critical ingredient in many theoretical treatments of these transitions, including, for example, analyses of osmotic stress, preferential hydration,[18] and cosolvent denaturation.[19]

The effects of pressure on solvation properties depend on the chemical groups of interest. For instance, pressure effects are different for polar versus nonpolar solutes in water.[20–22] Here, we focus on hydropbobicity, as it is a major driving force in biomolecular assembly processes such as protein folding,[23–37] though contributions from other types of driving forces can also be significant.[38–40] In this vein, previous computational efforts[41–43] have addressed pressure effects on the structure of water near a nonpolar solute, which may be monitored experimentally by neutron diffraction and isotopic substitution[44,45] as well as x-ray absorption spectroscopy.[46] A common general approach to relate volumetric and thermodynamic measurements to conformational properties of macromolecules is through experimental studies of solvation properties of small-molecule model compounds,[1,2,47] often by transferring them from a gas phase or a nonpolar liquid phase to an aqueous phase. As for many aspects of hydrophobic effects,[29,48] the rationale is based on the fact that conformational changes affect the solvent accessibility of various constituent chemical groups of a macromolecule. Thus, intuitively, it is plausible that the energetics of macromolecular conformational changes may be approximated by a summation of elementary solvation effects deduced from small-solute models of the constituent chemical groups.

This approach, which effectively considers single-solute solvation at infinite dilution, has led to numerous advances, and is the conceptual framework for the present simulation

[a)]Author to whom correspondence should be addressed. Tel.: +1-416-978-2697; Fax: +1-416-978-8548. Electronic mail: chan@arrhenius.med.toronto.edu

study. To put our work in a broader context, however, it should be recognized that the single-solute methodology, though useful as an important and necessary first step, would be ultimately limited because bulk hydrophobicity and "pair" hydrophobic interactions can be fundamentally different.[49] Indeed, recent atomic (explicit-water) simulations have shown that nonadditivity is significant for hydrophobic interactions among more than two nonpolar solutes.[50–52] More generally, the nature of hydrophobicity is length-scale dependent.[53–55] Consequently, some critical properties of the interactions among nonpolar groups in water are not captured by bulk-phase solvation and solvent accessible surface area analyses.[56] For certain intricate solvent effects in biomolecular processes,[57] even a rudimentary account requires the consideration of at least pairwise hydrophobic interactions. A prime example is the desolvation free energy barrier to the formation of a tight hydrophobic contact between two nonpolar solutes. Recently, this feature has been linked to the experimentally observed enthalpic barriers to protein folding,[58–60] as well as mutational effects on the activation enthalpy[61] and cooperativity[62] of folding kinetics. Another property associated with desolvation free energy barriers between small nonpolar solutes is a positive heat capacity change.[63–67] Notably, this intriguing phenomenon[68,69] provided rationalization for several otherwise puzzling behaviors of compact unfolded states of proteins,[70] even though such a positive heat capacity change was not predicted by bulk-phase solvent accessible surface area considerations.

For pressure effects, the relationship between properties of small-solute model compounds and that of macromolecular processes can be more subtle and even less understood. A well-known "paradox" is the opposite trend of pressure dependence between protein unfolding and the transfer of nonpolar groups from a liquid hydrocarbon solvent phase to water (which is expected to mimic unfolding):[24,71] Whereas the volume change tends to be positive at low pressures and negative at high pressures for protein unfolding, transfers of nonpolar groups from liquid hydrocarbons to water are associated with a volume decrease at low pressures and a volume increase at high pressures.

Atomic simulations have shed light on some of these puzzling phenomena. For instance, a study using the simple point charge water model and an information theory approach to extract properties of hydrophobic interactions from pure water simulations[72] has shown that, under increasing pressure, the solvent-separated configuration of two methanes becomes more favorable (has a less unfavorable potential of mean force) relative to the contact configuration.[73] Because the contact configuration is, aside from the contacting surface between the two methanes, well exposed to solvent, as has been discussed in the context of chemical and heat denaturations,[70] the above information-theory result[73] is relevant to the properties of pressure-unfolded protein conformations: It suggests that under high pressure, among protein conformations that are already unfolded, those that are more solvent exposed (corresponding to the solvent-separated two-methane configuration) are favored over partially solvated compact unfolded conformations that have higher degrees of hydrophobic burial. This scenario offers valuable insights into pressure denaturation of proteins, although a complete physical rationalization of the volumetric and compressibility differences between folded and unfolded states of proteins still awaits better accounts of hydrophobic interactions at larger length scales[53] and the contributions of void volumes in the packed cores of folded proteins.[2,74] Pressure effects on the association of two[75,76] and three[77] methanes, including their enthalpic and entropic aspects,[76,77] have also been addressed by direct simulations using the TIP3P (Refs. 76 and 77) and TIP4P (Ref. 75) water models. Recently, extensive explicit-water simulations have been conducted to study pressure and temperature effects on the folding/unfolding equilibrium of a 16-residue fragment of protein G,[78] a 20-residue predominantly α-helical (the "AK") peptide,[79] and a 20-bead freely jointed hydrophobic polymer chain,[80] as well as the compressibility of the folded states of several proteins.[74,81–83]

Despite these significant advances, there remain unanswered basic questions about pressure effects on hydrophobic hydration even at the single-solute, infinite dilution level. As emphasized by Kauzmann,[71] volume and enthalpy changes are equally fundamental to biomolecular processes. Compressibility as a derivative of volume is analogous to heat capacity as a derivative of enthalpy. For heat capacity, an increase in its value associated with nonpolar exposure is broadly observed experimentally in protein unfolding, model compound solvation, and in atomic simulations. In contrast, the corresponding picture for compressibility is less clear, partly because the effects of hydrophobic hydration on compressibility have not been well explored computationally thus far. An early simulation study of methane hydration under atmospheric pressure yielded an increase in compressibility (i.e., a positive partial molar compressibility).[42] But this prediction was opposite in sign to that deduced from experimental acoustic (sound velocity) measurements[6,7] on small model compounds.[1,2,21,84] On the other hand, experiments on pressure-induced protein unfolding showed that pressure-unfolded states *at high pressures* do have a higher compressibility than the folded states.[11] A coherent physical picture is lacking to rationalize these seemingly divergent trends.

Taking a basic step to address these questions, the present effort uses atomic simulation to examine the effects of pressure and temperature on hydration properties of a single methanelike solute, with an emphasis on the partial molar volume, compressibility, and heat capacity. The direct simulation approach adopted here is complementary to high-resolution analytical theories[85–88] and is critical for evaluating the physical basis, or lack thereof, of simplified statistical mechanical modeling approaches to pressure-dependent nonpolar solvation[89,90] and their macromolecular implications.[89,91] Previous simulations of the hydration heat capacity of methane[63–65,67] and xenon[66] were conducted under 1 atm. To our knowledge, pressure effects on single-solute hydration heat capacity (in contrast to heat capacity of hydrophobic interactions[92]) have not been computed using atomic simulation. Some of our simulations are for situations not yet accessible by current experimental techniques. To assess the reliability of our model, simulation results are

compared with experimental data in cases where the latter are available. For methane hydration, available experimental data include partial molar volume at several temperatures[93] (but not partial molar compressibility) and hydration heat capacity at a wide range of temperatures under 1 atm,[94,95] as well as for pressures up to ~280 atm.[96]

In addition to contributing to a foundation for the study of more complex many-body hydrophobic interactions, data on single-solute (infinite dilution) hydration under a broad range of pressure and temperature conditions are crucial by themselves for delineating solvation properties of open conformations in which individual constituent chemical groups are well exposed. Possible applications of this information range from advancing volumetric techniques as a general probe of biomolecular processes[16,17] to structural and functional studies of biomolecules from deep sea organisms living in high pressure environments.[97,98] As in studies under atmospheric pressure, single-solute hydration thermodynamic data[99,100] would be useful, for example, in providing physically appropriate heat capacity (calorimetric) base lines[101–103] to assess the effect of pressure on the cooperativity[52] of conformational transitions of RNA,[104] DNA,[105] and proteins.[106]

II. BASIC FORMULATIONS AND COMPUTATIONAL METHODS

Results in this report are obtained from constant-pressure, constant-temperature (*NPT*) Monte Carlo simulations of TIP4P water molecules[107,108] under a range of pressures from 1 to 3000 atm, and at eight different temperatures using BOSS version 4.1.[109] The temperatures used in our simulations are 278.15 K (5 °C), 288.15 K (15 °C), 298.15 K (25 °C), 308.15 K (35 °C), 318.15 K (45 °C), 328.15 K (55 °C), 348.15 K (75 °C), and 368.15 K (95 °C). For brevity, these temperatures will be referred to as, respectively, 278, 288, 298, 308, 318, 328, 348, and 368 K. A united-atom representation is used for methane. The size of the simulation box is subjected to variation in accordance with the constant-pressure constraint, and periodic boundary conditions are applied. Further details of the simulation methodology are provided in Ref. 63. The numerical parameters used in the present study are identical to that in the work of Shimizu and Chan.[56] In particular, the cutoff distance of water-water and water-methane interactions is 9.0 Å in our simulations.[63]

A. Test-particle insertion

At each pressure and temperature we study the hydration free energy of methane,

$$\Delta G = \mu_a^*, \tag{1}$$

where μ_a^* (pseudochemical potential[110]) is the Gibbs free energy of inserting a single methane into a given position in pure water and is obtained from simulation by using the relation[63]

$$\mu_a^* = -k_B T \ln\left[\frac{\langle V e^{-\beta U_a}\rangle_N}{\langle V\rangle_N}\right], \tag{2}$$

where $k_B T$ is Boltzmann's constant times absolute temperature, $\beta=(k_B T)^{-1}$, V is the volume of the system, and $\langle\cdots\rangle_N$ stands for averaging in the ensemble of N water molecules. Following the notation of Shimizu and Chan,[63] the average volume of the water molecules is defined analytically as

$$\langle V\rangle_N = \frac{\int dV V \int d\mathbf{r}_1 d\mathbf{r}_2 \cdots d\mathbf{r}_N e^{-\beta U_N} e^{-\beta PV}}{\int dV \int d\mathbf{r}_1 d\mathbf{r}_2 \cdots d\mathbf{r}_N e^{-\beta U_N} e^{-\beta PV}}, \tag{3}$$

where $\mathbf{r}_1, \mathbf{r}_2, \ldots, \mathbf{r}_N$ are the position vectors of the N water molecules, the potential energy U_N accounts for the interactions among the water molecules and is a function of their positions, and P is the pressure. The function U_a in Eq. (2) represents the interaction energy between the single methane and all of the water molecules. Clearly, $U_a = U_a(\mathbf{r}_a; \mathbf{r}_1, \mathbf{r}_2 \cdots \mathbf{r}_N)$, where $\mathbf{r}_a$ is the position vector of the inserted methane; but translational invariance of the solvent[48,110] implies that after averaging over water degrees of freedom the value of $\langle V e^{-\beta U_a}\rangle_N$ is independent of $\mathbf{r}_a$.

We apply test-particle insertion techniques[42,63,67] to compute the quantity in Eq. (2), noting that this technique is also well suited for the computation of potentials of mean force of two and more methanes.[67,111–113] For the study of single-methane hydration, we first use Monte Carlo sampling to generate a large collection of configurations of $N=395$ water molecules.[63] In each run, 1.5×10^5 initial (equilibrating) passes are discarded. Subsequently, coordinates (snapshots) of the water are collected every ten passes over a course of 2.1×10^7 passes. (In the present simulations, 1 pass equals to 395 Monte Carlo steps.) Subsequently, 10 000 insertions of a single methane are attempted per snapshot at different positions of the simulated box of water to estimate the ensemble averages in Eq. (2).

B. Partial molar volume from test-particle data

The partial molar volume per molecule, V_m, of methane in water may be estimated from the pressure dependence of μ_a^* from the following formulation. In the infinite dilution limit (i.e., when direct and solvent-mediated methane-methane interactions are negligible),

$$V_m = \langle V\rangle_{N+a} - \langle V\rangle_N, \tag{4}$$

where

$$\langle V\rangle_{N+a} = \frac{\int dV V \int d\mathbf{r}_a \int d\mathbf{r}_1 d\mathbf{r}_2 \cdots d\mathbf{r}_N e^{-\beta U_N} e^{-\beta U_a} e^{-\beta PV}}{\int dV \int d\mathbf{r}_a \int d\mathbf{r}_1 d\mathbf{r}_2 \cdots d\mathbf{r}_N e^{-\beta U_N} e^{-\beta U_a} e^{-\beta PV}} \tag{5}$$

is the average volume of N water molecules plus a single methane molecule. Making use of the fact that the expression

$$\int d\mathbf{r}_1 d\mathbf{r}_2 \cdots d\mathbf{r}_N e^{-\beta U_N} e^{-\beta U_a} e^{-\beta PV} \tag{6}$$

is independent of $\mathbf{r}_a$, the $\int d\mathbf{r}_a$ integrations in both the numeration and denominator of Eq. (5) merely yield a factor of V. Hence

$$\langle V\rangle_{N+a} = \frac{\int dV V^2 \int d\mathbf{r}_1 d\mathbf{r}_2 \cdots d\mathbf{r}_N e^{-\beta U_N} e^{-\beta U_a} e^{-\beta PV}}{\int dV V \int d\mathbf{r}_1 d\mathbf{r}_2 \cdots d\mathbf{r}_N e^{-\beta U_N} e^{-\beta U_a} e^{-\beta PV}}$$

$$= \frac{\langle V^2 e^{-\beta U_a}\rangle_N}{\langle V e^{-\beta U_a}\rangle_N} = \frac{\langle V^2\rangle_{N,a}}{\langle V\rangle_{N,a}}, \tag{7}$$

where $\langle\cdots\rangle_{N,a}$ here denotes averaging over water degrees of freedom with a single methane at a fixed position; i.e., $\langle\cdots\rangle_{N,a}=\langle\cdots e^{-\beta U_a}\rangle_N/\langle e^{-\beta U_a}\rangle_N$. It should be noted that the meaning of $\langle\cdots\rangle_{N,a}$ is different from that of $\langle\cdots\rangle_{N+a}$, as the latter does not fix the methane position and therefore entails averaging over the methane degrees of freedom as well.

We now consider the pressure derivative of μ_a^* while temperature is held constant. Using Eq. (3) and an analogous definition for $\langle V e^{-\beta U_a}\rangle_N$ in Eq. (2),

$$\Delta V \equiv \left(\frac{\partial \mu_a^*}{\partial P}\right)_T = \frac{\langle V^2\rangle_{N,a}}{\langle V\rangle_{N,a}} - \frac{\langle V^2\rangle_N}{\langle V\rangle_N}, \tag{8}$$

because $(\partial e^{-\beta PV}/\partial P)_T = -\beta V e^{-\beta PV}$. Hence, it follows from Eqs. (4) and (7) that the partial molar volume of methane per molecule

$$V_m = \Delta V + k_B T \kappa_T^0, \tag{9}$$

where

$$\kappa_T^0 = -\frac{1}{\langle V\rangle_N}\left(\frac{\partial\langle V\rangle_N}{\partial P}\right)_T = \frac{\beta}{\langle V\rangle_N}[\langle V^2\rangle_N - \langle V\rangle_N^2] \tag{10}$$

is the isothermal compressibility of pure water, and ΔV is termed the excess volume of solution. Equation (9) was provided in an earlier study of pressure effects in hydrophobic hydration by Matubayasi and Levy.[42] We shall refer to this procedure of obtaining V_m from μ_a^* as the indirect method of calculating partial molar volume. To clarify the physical meaning of ΔV vis-à-vis that of V_m, it is instructive to note that, in Eq. (8),

$$\frac{\langle V^2\rangle_N}{\langle V\rangle_N} = \langle V\rangle_N\left(1 + \frac{k_B T \kappa_T^0}{\langle V\rangle_N}\right) = \langle V\rangle_N[1 + O(N^{-1})], \tag{11}$$

because $\langle V\rangle_N$ increases essentially linearly with N. Similarly,

$$\frac{\langle V^2\rangle_{N,a}}{\langle V\rangle_{N,a}} = \langle V\rangle_{N,a}\left(1 + \frac{1}{\langle V\rangle_{N,a}}\left[\frac{\langle V^2\rangle_{N,a} - \langle V\rangle_{N,a}^2}{\langle V\rangle_{N,a}}\right]\right), \tag{12}$$

and the expression enclosed in square brackets in Eq. (12) approaches $k_B T \kappa_T^0$ in the infinite dilution limit because the effects of the single methane will be completely overwhelmed by contributions from an increasing number of water molecules as $N\to\infty$. Hence, $\lim_{N\to\infty}\langle V^2\rangle_{N,a}/\langle V\rangle_{N,a} = \langle V\rangle_{N,a}(1 + k_B T\kappa_T^0/\langle V\rangle_{N,a})$. Thus, it follows from Eq. (8) that in the infinite dilution limit,

$$\lim_{N\to\infty} \Delta V = \langle V\rangle_{N,a} - \langle V\rangle_N, \tag{13}$$

i.e., the excess volume would be exactly equal to the difference in volume between a very large box of water with a single methane *at a fixed position* and a corresponding box of pure water without the single methane, in line with common intuitive physical interpretations of "excess" quantities. It is important to recognize, nonetheless, that a finite (nonzero) difference [Eq. (9)] between the excess volume ΔV and the partial molar volume V_m [Eq. (4)] persists even in the $N\to\infty$ limit.

C. Direct determination of partial molar volume and compressibility

While the indirect method gives reasonable estimates of V_m (see below), it is not sufficiently sensitive to allow for reliable computation of compressibility, which requires values of V_m at different pressures (and therefore involves second derivatives of μ_a^* with respect to P). Thus, we have employed also an alternate technique to calculate V_m by directly determinating the volume distributions of two *NPT* simulation boxes: one containing 395 water molecules and a single methane at a fixed position,[114] and the other for pure water containing 395 water molecules. Volume data from the water plus methane simulation are used in conjunction with Eq. (7) to yield the first term on the right hand side of Eq. (4), whereas the average volume of the pure water simulation box is precisely the second term in Eq. (4). We will refer to this procedure of volumetric computation as the direct method. Direct simulations of volume distribution have been used by Jorgensen[115] and Matubayasi and Levy[42] to compute κ_T^0 for pure water. A direct method similar to the one employed here was used by Floris[116] to study excess volumes in hard-sphere solvation. Direct volume simulations have also been applied to study the compressibility of folded states of proteins.[74]

By definition,[117] the isothermal compressibility of our simulated water plus single methane system is given by

$$(\kappa_T)_a = -\frac{1}{\langle V\rangle_{N+a}}\left(\frac{\partial\langle V\rangle_{N+a}}{\partial P}\right)_T = \beta\left[\frac{\langle V^3\rangle_{N,a}}{\langle V^2\rangle_{N,a}} - \frac{\langle V^2\rangle_{N,a}}{\langle V\rangle_{N,a}}\right], \tag{14}$$

where the last equality follows from Eq. (7) linking $\langle V\rangle_{N+a}$ to the simulated $\langle\cdots\rangle_{N,a}$ averages with the methane at a fixed position. This expression for $(\kappa_T)_a$ corresponds to the isothermal compressibility of an aqueous solution of methane with solute mole fraction equals to N^{-1}. The related expression for the change of volume with respect to pressure $[(\kappa_T)_a$ without the $(\langle V\rangle_{N+a})^{-1}$ normalization]

$$(\mathcal{K}_T)_a \equiv -\left(\frac{\partial\langle V\rangle_{N+a}}{\partial P}\right)_T = \beta\left[\frac{\langle V^3\rangle_{N,a}}{\langle V\rangle_{N,a}} - \left(\frac{\langle V^2\rangle_{N,a}}{\langle V\rangle_{N,a}}\right)^2\right] \tag{15}$$

will be useful as well for the consideration of partial molar or excess compressibility below. This quantity is sometimes referred to also as "isothermal compressibility" in the biophysics literature (see, e.g., Ref. 7).

The effects of methane hydration on solution compressibility are provided by comparing Eqs. (10), (14), and (15). The difference between $(\kappa_T)_a$ [Eq. (14)] and κ_T^0 in [Eq. (10)],

$$(\kappa_T)_a - \kappa_T^0 = \left(\frac{\partial \kappa_T}{\partial n}\right)_{P,T}, \tag{16}$$

where n denotes the number of methanes, is the change in isothermal compressibility, relative to that of pure water, caused by the addition of methane to water at mole fraction N^{-1}. Here we have introduced the notation κ_T which is the isothermal compressibility of a general aqueous solution of methane and thus a function of n. Conforming to common usage in biophysics,[7,16] we define the partial molar isothermal compressibility as

$$\mathcal{K}_T^o = \left(\frac{\partial \mathcal{K}_T}{\partial n}\right)_{P,T} = -\left(\frac{\partial V_m}{\partial P}\right)_T = -\left(\frac{\partial \langle V\rangle_{N+a}}{\partial P}\right)_T - \left[-\left(\frac{\partial \langle V\rangle_N}{\partial P}\right)_T\right], \tag{17}$$

where V_m is the partial molar volume, and $\mathcal{K}_T = -(\partial\langle V\rangle/\partial P)_T$ is the negative pressure derivative of the volume of a general aqueous solution of methane; $\mathcal{K}_T^o$ is the change caused by a methane to the rate of volume decrease per unit increase in pressure. We compute $\mathcal{K}_T^o$ in the infinite dilution limit using the above formulation derived from the basic expressions in Eqs. (3)–(5) for V_m. A closely related "excess compressibility" was defined by Matubayasi and Levy[42] as

$$\Delta\kappa_T = -\rho^0\left(\frac{\partial \Delta V}{\partial P}\right)_T = -\rho^0\left(\frac{\partial^2 \mu_a^*}{\partial P^2}\right)_T, \tag{18}$$

where ΔV is the excess volume [see Eq. (9)] and $\rho^0 = N/\langle V\rangle_N$ is the number density of the pure solvent. Conceptually, $\Delta\kappa_T$ may be more suited to applications in which compressibility contributions from the solute translational degrees of freedom should be excluded, though in practice $\Delta\kappa_T$ often does not differ much from $\rho^0\mathcal{K}_T^o$.

III. RESULTS AND DISCUSSION

A. *NPT* ensembles of pure water

To set up a necessary basis for understanding the effects of hydrophobic hydration, we first examine pertinent properties of pure water. Figure 1 shows simulated pure water density at two temperatures as functions of pressure as well as the corresponding experimental data from the National Institute of Standards and Technology (NIST).[118] The results indicate that for a given temperature, the TIP4P model is quite adequate in capturing the trend of density increase with increasing pressure, i.e., the isothermal compressibility, of pure water, although the simulated isothermal compressibilities appear to be slightly higher (have slightly higher ρ^0 vs P slopes) than their experimental counterparts.

Figure 2 (upper panel) shows the temperature dependence of water density at different pressures. Comparisons with the plotted experimental data indicate that while the TIP4P model exhibits a trend generally similar to the experimental trend, the model predicts density increases with temperature (ρ^0 vs T slopes) that are about two times that of the corresponding experimental values,[119] as has been documented previously.[66] From a quadratic fit (see Fig. 2), our simulation data at 1 atm predict an isobaric thermal expansitivity of pure water $\alpha^0 = (\partial\langle V\rangle_N/\partial T)_P/\langle V\rangle_N = 5.64 \times 10^{-4}$ K^{-1} under atmospheric pressure. This is essentially identical, as it should, to the $\alpha^0 = 5.67 \times 10^{-4}$ K^{-1} value one may compute from the polynomial fit to the TIP4P model data in the work of Paschek[66] (Table III of this reference). Although the TIP4P model predictions for α^0 are significantly higher than the experimental value of 2.572×10^{-1} K^{-1} from Kell,[119] the similarity in curvature of the theoretical and experimental curves for 1 atm in the upper

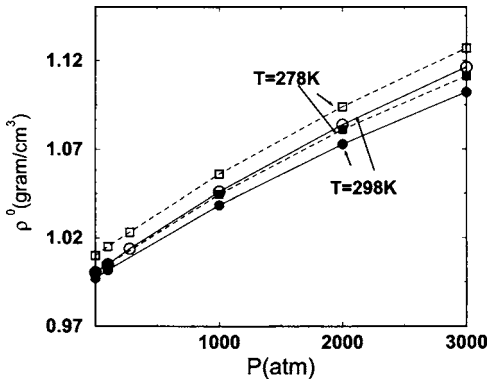

FIG. 1. Mass density of pure water as a function of pressure at 278 (squares) and 298 K (circles). In this and all subsequent figures in this paper, the lowest pressure for which data are presented is $P=1$ atm. Our simulation results (open symbols) computed using 395 TIP4P water molecules are compared with experimental data (filled symbols) from NIST (Ref. 118). The solid and dashed lines joining the data points are a guide for the eye.

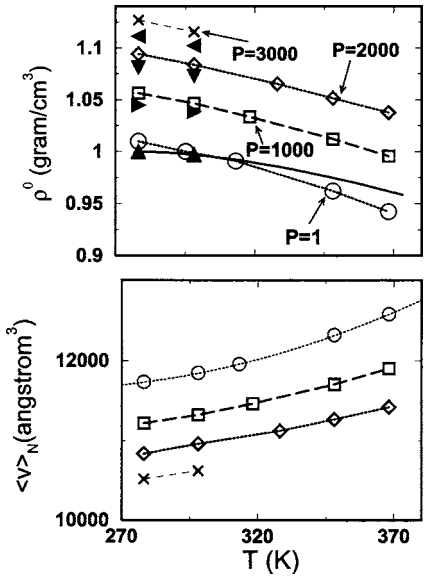

FIG. 2. The temperature dependence of model mass density (upper panel) and average volume (lower panel) of pure water simulated using 395 TIP4P water molecules are given for pressure (P in atm)=1 (circles), 1000 (squares), 2000 (diamond), and 3000 (crosses). Fitted curves through the simulated data points are a guide for the eye. For $P=1$ atm in the lower panel, the continuous curve is given by the least-square fit $\langle V\rangle_N = 1.463 \times 10^4 - 25.37T + 0.053\,75T^2$. In the upper panel, experimental data from NIST (Ref. 118) at the four pressures (filled symbols), and from Kell (Ref. 119) for $P=1$ atm (thick continuous curve) are included for comparison.

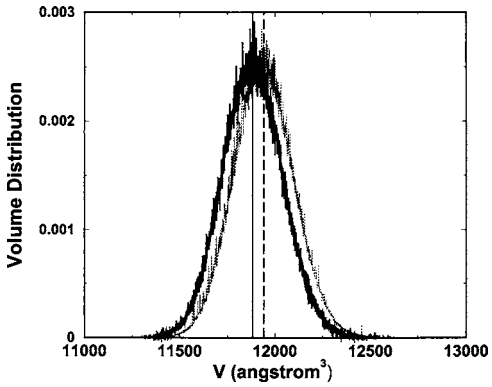

FIG. 3. The volume distribution simulated using the TIP4P model at $P=1$ atm and $T=298$ K for a box of $N=396$ water molecules (darker trace) is compared to that for a box with the same number of water molecules plus a stationary methane (lighter trace). Their average (mean) volumes are, respectively, $\langle V\rangle_N=11\,883.3$ Å^3 and $\langle V\rangle_{N,a}=11\,940.9$ Å^3 (marked by vertical solid and dashed lines); thus the excess volume $\langle V\rangle_{N,a}-\langle V\rangle_N=57.6$ Å^3. A bin size of 1 Å is used for the distributions. The distribution value plotted at a given V corresponds to the probability that the volume of the simulated system is $\geqslant V$ but $<V+1$ Å^3.

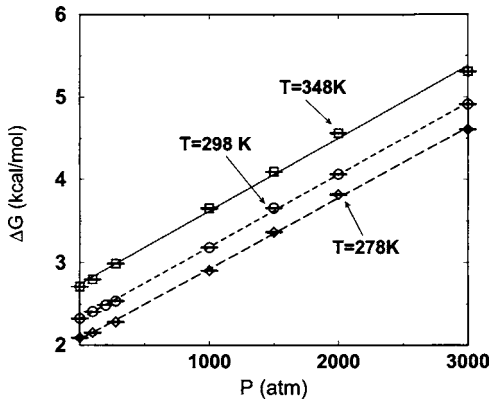

FIG. 4. Simulated hydration free energy ΔG of methane determined using test-particle insertion techniques under a range of pressures at three temperatures. The error bars indicate statistical uncertainties estimated from block averages. The straight lines are least-square fits.

panel of Fig. 2 indicates that the theoretical temperature derivative of isobaric expansitivity, $(\partial\alpha^0/\partial T)_P$, is well predicted by the TIP4P model. Indeed, the quadratic fit to our simulated data gives $(\partial\alpha^0/\partial T)_P=8.8\times10^{-6}$ K^{-2} under atmospheric pressure. This theoretical result is in reasonable agreement with the corresponding experimental value of 9.6×10^{-6} K^{-2} provided by Kell.[119]

B. Partial molar volume of methane in water

We now turn to the volumetric effects of nonpolar hydration. Figure 3 compares the directly simulated distribution of total volume of pure water to that of a single methane with the same number of water molecules, both at the same room temperature and under atmospheric pressure. The two distributions mostly overlap with each other, consistent with a significant probability of methane-size cavities in pure water under these conditions.[72] Using Eq.(10) and the simulated pure water distribution in Fig. 3, we obtain $\kappa_T^0=5.13\times10^{-5}$ atm^{-1}, in reasonable agreement with the experimental value of 4.588×10^{-5} atm^{-1} from Kell.[119] Applying the formalism in Sec. II B to our pure water and methane plus water volume distribution data yields an excess volume of methane hydration $\Delta V=57.6$ Å^3 [$\Delta V=57.61$ Å^3 according to Eq. (8) or 57.63 Å^3 from Eq. (13) for the infinite dilution limit]. Therefore, using Eq. (9) and our simulation results for κ_T^0 and ΔV, the partial molar volume of methane hydration at 298 K and 1 atm we computed using the TIP4P model is $V_m=59.7$ Å^3 (equivalent to 36.0 cm^3 mol^{-1}), in good agreement with an experimental value of $\approx$37.2 cm^3 mol^{-1} from Masterton.[93]

Figure 4 shows the pressure dependence of hydration free energy of one methane at three temperatures for pressures ranging from 1 to 3000 atm. As pressure increases, ΔG increases: insertion of methane into water becomes more difficult at higher pressures as the water becomes denser (Fig. 2). Following Eq. (8), the excess volume of methane hydration may be computed from the slopes in Fig. 4 (the indirect method in Sec. II B). However, a reliable estimate of compressibility is not possible from these ΔG vs P plots because the curvature is difficult to discern. Therefore, for each temperature, we attempted only a single linear fit over the entire pressure range and the resulting excess volume is taken to be representative of that under pressures in the simulated range. For $T=298$ K, a least-square linear fit to the simulated data points gives $\Delta V=36.4$ cm^3 mol^{-1}. If we apply Eq. (9) with the $\kappa_T^0=5.13\times10^{-5}$ atm^{-1} value above from direct volume distribution simulation together with the $\Delta V=36.4$ cm^3 mol^{-1} from $(\partial\Delta G/\partial P)_T$ in Fig. 4, we obtain a partial molar volume of $V_m=36.4+1.3=37.7$ cm^3 mol^{-1}, which agrees very well with our directly simulated value and experimental data[93] for 1 atm, as discussed above. Our calculated ΔV values from both the direct (Fig. 3) and indirect pressure-derivative (Fig. 4) methods are also in reasonable agreement with a calculated value of 35.1 cm^3 mol^{-1} for $\approx$1 atm in an earlier TIP4P model study.[42]

C. Pressure and temperature dependence of hydration free energy

The temperature dependence of the simulated ΔG in Fig. 5 for several pressures all exhibit curvatures characteristic of

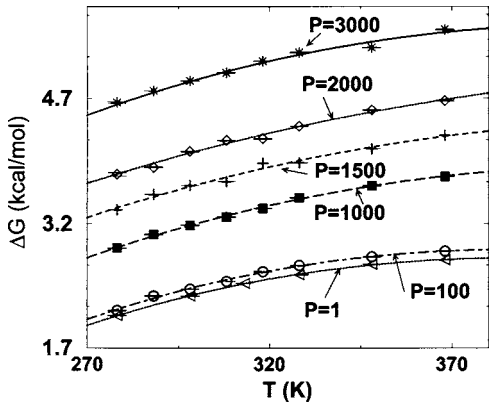

FIG. 5. Temperature dependence of simulated hydration free energy ΔG of methane under different pressures (P in atm). The error bars indicate statistical uncertainties estimated from block averages. The continuous curves are least-square fits using Eq. (19).

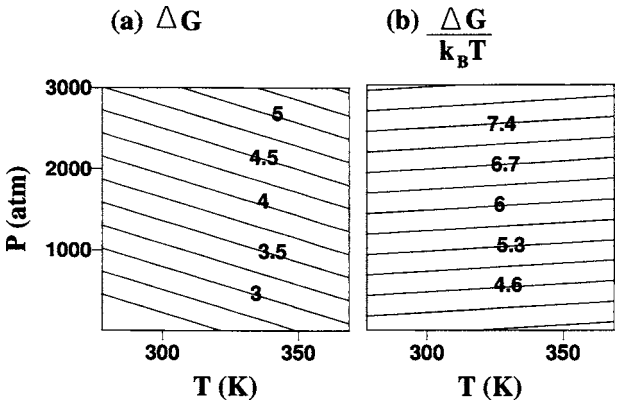

FIG. 6. Contour plots of the simulated methane hydration free energy ΔG in kcal mol^{-1} (a) and $\Delta G/k_BT$ (b) as functions of pressure P and temperature T. The plots were constructed from our simulated data in Figs. 4 and 5 using the software "SURFER8—Contouring and 3D Surface Mapping for Scientists and Engineers" (Golden Software Inc., Golden, Colorado).

hydrophobic hydration. To ascertain the effects of pressure on the enthalpy, entropy, and heat capacity of nonpolar hydration, the simulated free energies are fitted to the relation

$$\mu_a^* = \Delta G(P) = \Delta H_0(P) + (T - T_0)\Delta C_P(P) - T\Delta S_0(P) - T\Delta C_P(P)\ln\left(\frac{T}{T_0}\right), \quad (19)$$

as in previous studies[63,67] at 1 atm. Here $\Delta H_0(P)$ and $\Delta S_0(P)$ are hydration enthalpy and entropy, respectively, at a given reference temperature T_0 and pressure P, and $\Delta C_P(P)$ is the constant-pressure hydration heat capacity, which, as a first approximation, is taken to be temperature independent at a given P.

The variation of hydration free energy ΔG of methane as a function of temperature and pressure (data in Figs. 4 and 5) is summarized in the contour plot in Fig. 6(a). The contour plot in Fig. 6(b) is for the corresponding dimensionless $\Delta G/k_BT$ value, which is proportional to the Flory χ interaction parameter in polymer theories.[91,120,121] These contour plots show that exposing a small nonpolar solute to water is strongly disfavored by increasing pressure. This basic observation indicates that single-solute bulk-phase solvation properties of small nonpolar solutes are insufficient by themselves to rationalize pressure denaturation of proteins,[16,17] because, intuitively, the results in Fig. 6 would suggest that folding (which entails burial of nonpolar surfaces and therefore less nonpolar exposure), rather than unfolding, would be favored by higher pressures. In other words, it would suggest pressure stabilization of the folded state instead of pressure denaturation. In this regard, it is noteworthy that whereas semiquantitative aspects of heat[120] and chemical[121] denaturation, of protein may be rationalized by directly applying experimental bulk-phase transfer data[120,121] to mean-field heteropolymer models,[122] pressure-dependent properties of experimental bulk-phase transfers cannot be and were not used directly to rationalize pressure denaturation in similar mean-field modeling.[91]

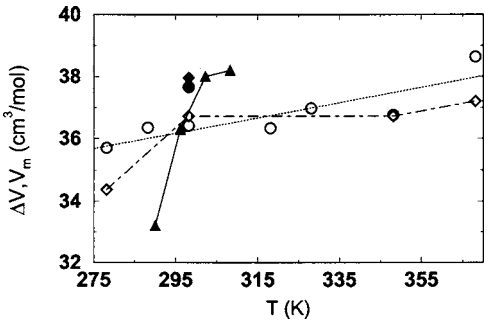

FIG. 7. Estimating the partial molar thermal expansitivity of methane in water. Volume changes upon insertion of a single methane at $P=1$ atm are computed in the TIP4P water model at several temperatures using the indirect $(\partial\Delta G/\partial P)_T$ method (circles) as well as the direct volume simulation method (diamonds). The computed excess volumes (ΔV) are given by the open symbols. The corresponding partial molar volumes (V_m) are obtainable by Eq. (9) using the directly simulated κ_T^0, and are shown by the filled symbols, as an example, for 298 K. The filled triangles are experimental V_m values of methane in water determined by Masterton (Ref. 93). Volume changes are given in units of cm^3/mol (1 Å^3 per methane molecule $=0.602\,214$ cm^3/mol of methane). The dotted inclined straight line is the least-square fit to the ΔV values calculated using the indirect method. Data points from experiments and direct simulations are joint by solid and dashed lines, respectively, as a guide for the eye.

D. Isobaric expansitivity

Continuing our systematic analysis of methane hydration, the temperature dependence of the excess and partial molar volume of methane in water is studied in Fig. 7. Here, as a first step, we restrict our consideration to 1 atm, for which some experimental data[93] are available for comparison. We have calculated theoretical excess volumes by both the indirect pressure-derivative method (using the data in Fig. 5) and direct simulations of mean volumes at four temperatures [Eq. (13), $N=395$]. Partial molar volumes differ from the corresponding excess volumes by $k_BT\kappa_T^0$ [Eq. (9)]. Theoretical partial molar volumes are provided for $T=298$ K in Fig. 7 using the simulated κ_T^0 at this temperature (see above). Although we have not calculated theoretical κ_T^0 values for other T's, the difference between theoretical V_m and ΔV is expected to be similar for other temperatures in this figure. This is because the TIP4P model is apparently capable of reproducing experimental isothermal compressibilities of pure water at different temperatures with reasonable accuracies (Fig. 1), and all of the experimental κ_T^0 values[119] at 1 atm from $T=273$ to 373 K are $\sim 5\times10^{-5}$ atm^{-1} [$\kappa_T^0=(4.48-5.16)\times10^{-5}$ atm^{-1}] and therefore the upshift of V_m from ΔV varies only between ~ 1.2 and 1.5 cm^3 mol^{-1} and does not change significantly for the entire temperature range for liquid water under atmospheric pressure. Hence, $(\partial V_m/\partial T)_P \approx (\partial\Delta V/\partial T)_P$.

Our computational results from both the direct and indirect methods exhibit an increase in ΔV with increasing T. The ΔV estimated from the indirect method increases more or less gradually with increasing T, ranging from ≈ 36 cm^3 mol^{-1} at 278 K to ≈ 39 cm^3 mol^{-1} at 368 K. On the other hand, the ΔV estimated using direct volume simulation shows a significant increase from ≈ 34 cm^3 mol^{-1} at 278 K to ≈ 37 cm^3 mol^{-1} at 298 K before leveling off for higher temperatures. Although the trends obtained from the

two methods are not identical, together, these model predictions of a general trend of $(\partial \Delta V/\partial T)_P \approx (\partial V_m/\partial T)_P > 0$ are consistent with experiments.[20,93] Thus, it underscores that in this particular respect atomic modeling is more successful than a recent insightful lattice model of hydrophobic effect[90] that predicted a decreasing partial molar volume of methane in water with increasing T.

Experimentally determined partial molar volumes of methane in water are available from Masterton[93] for a limited temperature range. These experimental data (triangles in Fig. 7) show a rather dramatic temperature dependence of V_m under constant atmospheric pressure: V_m increases rapidly with T at lower temperatures (<300 K) then almost levels off when T reaches a higher temperature ~310 K. This phenomenon implies that methane significantly increases the isobaric expansitivity of the aqueous solution at lower temperatures $[(\partial V_m/\partial T)_P \approx (\partial \Delta V/\partial T)_P \approx 0.27\ \mathrm{cm^3\ mol^{-1}\ K^{-1}}$ at 298 K] but have a much smaller or even negligible effect at higher temperatures. Remarkably, the ΔV values we obtained from direct volume simulations show a similar trend of rapid increase with T at low T followed by a leveling off at high T, though the computed rate of increase at low T $[(\partial V_m/\partial T)_P \approx (\partial \Delta V/\partial T)_P \approx 0.12\ \mathrm{cm^3\ mol^{-1}\ K^{-1}}$ at 298 K] is not as high as that observed experimentally. Because the direct simulation method does not involve pressure derivatives and does not rely on averaging over different pressures, we expect it to be more accurate for determining volumes at a given pressure than the indirect method. In this light, the fact that the experimental temperature dependence of V_m of methane is qualitatively similar to our direct simulation results suggests that the physics of the experimental $V_m(T)$ trend is at least partly captured by the present model with TIP4P water molecules.

Interestingly, our direct simulation result stipulating a large and positive $(\partial V_m/\partial T)_P$ at temperatures around and lower than 298 K is qualitatively consistent not only with direct experimental measurements on methane[93] but also with the general trend Kharakoz[20] extracted from a compilation of experimental data on various aliphatic compounds. For instance, according to Kharakoz's fitted linear relationship between $(\partial V_m/\partial T)_P$ and solvent accessible surface area (SASA) at 25 °C for aliphatic compounds (Fig. 3 of Ref. 20), the $(\partial V_m/\partial T)_P$ of an aliphatic molecule with a SASA $\approx 1.37\ \mathrm{nm^3}$ equal to that of methane is predicted to be $\approx 0.06\ \mathrm{cm^3\ mol^{-1}\ K^{-1}}$.

E. Isothermal compressibility

We now investigate in more detail the pressure dependence of volume changes associated with methane hydration at room temperature (298 K). For this purpose, we use the direct method in Sec. II C because the indirect method in Sec. II B does not offer statistically reliable estimates for the desired quantities, which are second derivatives of the free energy with respect to pressure. Figure 8 shows the pertinent average volumes obtained by direct simulation at four pressures. It is evident from these data that the volume of pure water and the volume of the methane plus water system both

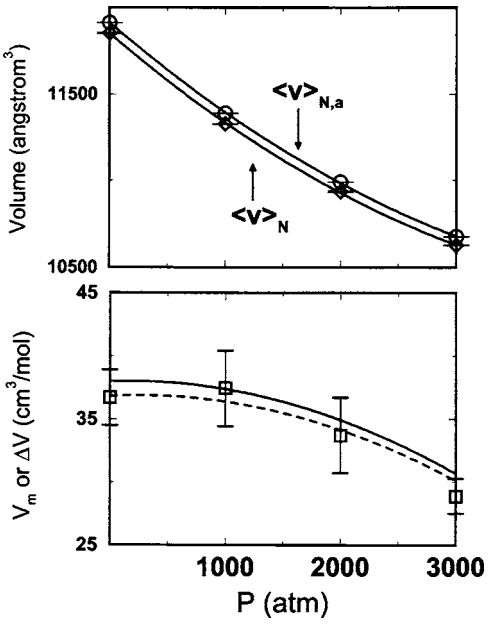

FIG. 8. Pressure dependence of partial molar volume and isothermal compressibility at $T=298$ K. Upper panel: Average volume $\langle V\rangle_N$ (diamonds) for 395 water molecules and $\langle V\rangle_{N,a}$ (circles) for one stationary methane molecule plus 395 water molecules were determined by direct simulations at four different pressures, $P=1$, 1000, 2000, and 3000 atm. Continuous curves through the simulated data points are least-square quadratic fits for the pressure-dependent volumes (see text). Lower panel: excess volume ΔV (squares) is equal to the difference $\langle V\rangle_{N,a}-\langle V\rangle_N$. The dashed curve is ΔV from the volume fits. The solid curve is the partial molar volume V_m obtained from the fitted ΔV using Eq. (9) and κ_T^0 values determined from the same fits. The error bars represent sampling uncertainties estimated from block averages. The volumes in the upper panel are in $\mathrm{Å^3}$, whereas the volumes in the lower panel are reported in $\mathrm{cm^3/mol}$ to facilitate comparisons with experimental data. Note that the average volumes at $P=1$ atm in the upper panel are different from that in Fig. 3 because the results in the present Fig. 8 were simulated using 395 instead of 396 water molecules. Here, $\langle V\rangle_N = 11\,850.3\ \mathrm{Å^3}$ and $\langle V\rangle_{N,a} = 11\,911.2\ \mathrm{Å^3}$ at 1 atm. The resulting excess volume $\langle V\rangle_{N,a}-\langle V\rangle_N = 60.9\pm 3.7\ \mathrm{Å^3}$ is consistent with that deduced from Fig. 3, as it should.

have a nonlinear dependence on pressure. Thus, as a first approximation, we employ fitting equations quadratic in pressure

$$\langle V\rangle_N = a_0 + b_0 P + c_0 P^2, \quad \langle V\rangle_{N,a} = a_1 + b_1 P + c_1 P^2, \quad (20)$$

to extract volumetric and compressibility information from the multiple-pressure simulation data in the upper panel of Fig. 8. From Eq. (20), we may calculate, for example, $-(\partial \langle V\rangle_N/\partial P)_T = -(b_0 + 2c_0 P)$ and therefore determine the isothermal compressibility of pure water as $\kappa_T^0 = -(b_0 + 2c_0 P)/(a_0 + b_0 P + c_0 P^2)$, and derive analogous relations using the parameters fitted to $\langle V\rangle_{N,a}$ for the methane plus water system. Least-square fitting of the simulated average volumes in Fig. 8 leads to $a_0 = 11\,848.4 \pm 11.1\ \mathrm{Å^3}$, $b_0 = -0.566\,29 \pm 0.017\,86\ \mathrm{Å^3\ atm^{-1}}$, $c_0 = (5.3117 \pm 0.5703) \times 10^{-5}\ \mathrm{Å^3\ atm^{-3}}$ and $a_1 = 11\,909.6 \pm 9.1\ \mathrm{Å^3}$, $b_1 = -0.565\,55 \pm 0.014\,69\ \mathrm{Å^3\ atm^{-1}}$, $c_1 = (5.1623 \pm 0.4690) \times 10^{-5}\ \mathrm{Å^3\ atm^{-2}}$. To study pressure dependence in the analysis below, we use these multiple-pressure fitted parameters to calculate compressibilities and other pressure and temperature derivatives of volume instead of calculating them solely from the volume distribution at a given pressure as in Fig. 3.

This is because the numerical convergence of mean values is generally much more efficient than that of higher moments,[115] even though overall convergence tends to be inefficient at high pressures.

Substituting these multiple-pressure fitted parameters into the above formula for isothermal compressibility of pure water gives $\kappa_T^0=4.78\times10^{-5}$ atm^{-1} at 1 atm. The methane excess volume ΔV at 1 atm is also computed using the fitted parameters in conjunction with Eqs. (8) and (13), yielding essentially identical results—61.19 and 61.20 Å^3, respectively, for the two formulas. Hence, from Eq. (9), the partial molar volume of methane V_m predicted by the fitted parameters equals 63.1 Å^3 at 1 atm. We note that these V_m and κ_T^0 values deduced from fitting the mean volumes at multiple pressures in Fig. 8 differ only slightly, and thus are consistent—as they should—with the corresponding values of 59.7 Å^3 and 5.13×10^{-5} atm^{-1} computed solely from the 1 atm volume distributions in Fig. 3.

The lower panel of Fig. 8 indicates an increase in partial molar volume when pressure is raised from $P=1$ to 1000 atm. Although more extensive sampling may be needed to ascertain this feature in view of the numerical uncertainties (error bars in the figure), for pressures $P>1000$ atm there is a definitive trend of decreasing partial molar volume with increasing pressure. Numerical uncertainties notwithstanding, it is also clear that this decrease is nonlinear in that the rate of decrease quickens with increasing pressure. The existence of a maximum excess and partial molar volumes of methane at ~1000 atm implies that the excess and partial molar isothermal compressibilities would be negative at low pressures. Using the above fitting parameters, the excess isothermal compressibility $\Delta\kappa_T$ in Eq. (18) at $P=1$ atm is given by $\Delta\kappa_T/\rho^0=-(\partial\Delta V/\partial P)_T=-7.48\times10^{-4}$ Å^3 atm^{-1} $(-4.50\times10^{-4}$ cm^3 mol^{-1} atm$^{-1})$. By Eq. (9), the corresponding partial molar isothermal compressibility in Eq. (17) at 1 atm is $\mathcal{K}_T^o=-(\partial V_m/\partial P)_T=\Delta\kappa_T/\rho^0-k_BT(\partial\kappa_T^0/\partial P)_T$, where $(\partial\kappa_T^0/\partial P)_T$ is now given by $-2c_0/(a_0+b_0P+c_0P^2)+(b_0+2c_0P)^2/(a_0+b_0P+c_0P^2)^2$, yielding $\mathcal{K}_T^o=-4.77\times10^{-4}$ Å^3 atm^{-1} $(-2.87\times10^{-4}$ cm^3 mol^{-1} atm$^{-1})$.

Consistent with these trends, the partial molar isothermal compressibility computed directly from the 1 atm volume distributions in Fig. 3 is equal to $\mathcal{K}_T^o=-1.84\times10^{-3}$ Å^3 atm^{-1} $(-1.11\times10^{-3}$ cm^3 mol^{-1} atm$^{-1})$, which is also negative, and even more so than the above $\mathcal{K}_T^o$ value computed from the multiple-pressure fit in Fig. 8. In this regard, we note that in the lower panel of Fig. 8, the fitted dashed curve for ΔV passes below the simulated data points at 1000 atm. Now, if the difference between the simulated ΔV values (squares) at 1 and 1000 atm in this figure is used to approximate the pressure dependence at 1 atm, one would obtain, for 1 atm, $(\partial\Delta V/\partial P)_T\approx-9.0\times10^{-4}$ cm^3 mol^{-1} atm^{-1}; hence (as in the last paragraph) $\mathcal{K}_T^o\approx-7.4\times10^{-4}$ cm^3 mol^{-1} atm^{-1}, which is of the same order is the above $\mathcal{K}_T^o=-1.11\times10^{-3}$ cm^3 mol^{-1} atm^{-1} computed directly from Fig. 3. Taken together, these observations suggest quite strongly that the present model with TIP4P water may indeed entail a 1-atm $\mathcal{K}_T^o$ significantly more negative than the -2.87×10^{-4} cm^3 mol^{-1} atm^{-1} value we have obtained from multiple-pressure fits.

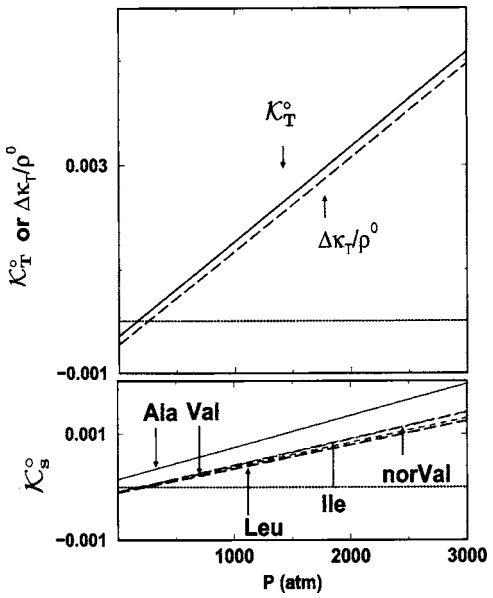

FIG. 9. Partial molar and excess compressibilities of methane in water increase with pressure. Upper panel: theoretical isothermal partial molar and excess compressibilities of methane calculated from the volume fits in Fig. 8 (see text for formulation). Both $\mathcal{K}_T^0$ and $\Delta\kappa_T/\rho^0$ are negative at atmospheric pressure ($P=1$ atm) but become positive for $P>\sim250$ atm. Lower panel: experimental partial molar adiabatic compressibility of a methyl or a methylene group, estimated from the data of Sarvazyan and Chalikian (Ref. 84) on six amino acids' adiabatic compressibilities and their rates of change with respect to pressure (Table 1 of Ref. 84). Here, the lines labeled by Ala, Val, norVal, Ile, and Leu are, respectively, 1, 1/3, 1/3, 1/4, and 1/4 times the quantity that equals to the measured partial molar adiabatic compressibility of alanine, valine, norvaline, isoleucine, and leucine minus that of glycine. Compressibilities (vertical axes) are in units of cm^3 mol^{-1} atm^{-1}.

In contrast, in an earlier study, Matubayasi and Levy[42] reported a positive $\Delta\kappa_T=(3.3\pm2.6)\times10^{-3}$ atm^{-1} for a methane in TIP4P water with mass density of 1.0 g cm^{-3} at 10 °C ($P\approx1$ atm). Their result implies that $-(\partial\Delta V/\partial P)_T=\Delta\kappa/\rho^0=(5.9\pm4.7)\times10^{-2}$ cm^3 mol^{-1} atm^{-1} (because $\rho^0=0.0556$ mol cm^{-3}), which is opposite in sign to, and much larger in magnitude than the present results for $\Delta\kappa_T/\rho^0$ at 25 °C and 1 atm. However, the methane excess compressibility predicted by these authors[42] appears to be unreasonably high because it is nearly two orders of magnitude larger than the corresponding $-(\partial\Delta V/\partial P)_T$ value of $\sim9\times10^{-4}$ cm^3 mol^{-1} atm^{-1} for pure water.[123]

While the isothermal compressibilities of both pure water and the methane plus water systems decrease with increasing pressure (volume versus pressure slopes become less negative in the upper panel of Fig. 8), as stated above the trend in the lower panel of Fig. 8 implies that the *excess* and *partial molar* isothermal compressibilities of methane increase with increasing pressure at high pressures. This is depicted quantitatively in the upper panel of Fig. 9, which shows a crossover from negative to positive values of excess or partial molar isothermal compressibility at $P\sim100-250$ atm. In other words, under isothermal conditions, our model predicts that exposing a small nonpolar solute to water at room temperature makes the solution less

compressible at low pressures (i.e., one to several hundred atmosphere), but would produce an opposite effect of making the solution more compressible at high pressures. Figuratively speaking, our results suggest that "hydrophobic water" is "hardened" (relative to pure water) at low pressures but "softened" at high pressures. Inasmuch as protein unfolding entails increased exposure of hydrophobic groups, our predicted trend is consistent with the increase in isothermal compressibility of pressure-induced protein unfolded states (reviewed in Ref. 16) under high pressures (e.g., ~500–1000 atm in a study on staphylococcal nuclease[11]) relative to that of the stable folded state at lower pressures. Thus, with further in-depth analyses, our results should contribute to a physical understanding of this experimental phenomenon.

F. Adiabatic compressibility

To our knowledge, the partial molar compressibility of methane has not been determined experimentally. Nonetheless, acoustic measurements on aqueous solutions of model compounds indicate that the contribution of a methyl or methylene group to partial molar adiabatic (isentropic) compressibility is negative at room temperature under atmospheric pressure,[2,21,84] but the contribution increases with pressure and becomes positive at higher pressures.[84] This experimental trend of partial molar adiabatic compressibility (see examples provided in the lower panel of Fig. 9)[124] is remarkably similar to our theoretically predicted partial molar isothermal compressibility of methane in water (upper panel of Fig. 9), hinting that the present model results may be consistent with existing experimental data, even though the theoretical and experimental compressibilities are determined under different conditions.

To delineate the implications of our results on partial molar adiabatic compressibilities, we note that the relationship between isothermal and adiabatic compressibilities follows from the basic thermodynamic identities

$$\left(\frac{\partial V}{\partial P}\right)_S = \left(\frac{\partial V}{\partial P}\right)_T + \left(\frac{\partial V}{\partial T}\right)_P \left(\frac{\partial T}{\partial P}\right)_S, \tag{21}$$

and $(\partial T/\partial P)_S = -(\partial S/\partial P)_T/(\partial S/\partial T)_P$. Making use of the fact that the constant-pressure heat capacity $C_P = T(\partial S/\partial T)_P$, and applying the Maxwell relation $(\partial S/\partial P)_T = -(\partial V/\partial T)_P$, Eq. (21) may be rewritten in the familiar form[6,119]

$$-\left(\frac{\partial V}{\partial P}\right)_S = -\left(\frac{\partial V}{\partial P}\right)_T - \frac{T}{C_P}\left[\left(\frac{\partial V}{\partial T}\right)_P\right]^2. \tag{22}$$

The physical meaning of this general relation is as follows. Because temperature can change in an adiabatic process, the difference between adiabatic and isothermal compressibilities originates from the adiabatic temperature change. Equation (22) shows that, provided $C_P > 0$ and $(\partial V/\partial T)_P > 0$, as is the case for many systems, volume contracts less when compressed adiabatically than when compressed isothermally because adiabatic temperature increase tends to increase volume. The magnitude of the difference in compressibility is inversely proportional to heat capacity. That is, the adiabatic-isothermal compressibility difference is larger when less energy is needed to increase the temperature of the system. The difference is also quadratic in the rate of volume increase with respect to temperature. In other words, the adiabatic-isothermal compressibility difference is larger when the system is thermally more expansible, as one would intuitively expect.

It follows from Eq. (22) that the adiabatic excess compressibility, $\Delta\kappa_S$, is given by

$$\Delta\kappa_S = \Delta\kappa_T - \rho^0\left\{ \frac{T}{C_P}\left[\left(\frac{\partial V}{\partial T}\right)_P\right]^2\Big|_{N,a} - \frac{T}{C_P}\left[\left(\frac{\partial V}{\partial T}\right)_P\right]^2\Big|_N \right\}, \tag{23}$$

where $\rho^0 = N/\langle V\rangle_N$, and the first and second of the two terms enclosed in curly brackets are evaluated for the systems, respectively, of a fixed methane in water and a box of pure water, as defined above. Hence,

$$\frac{T}{C_P}\left[\left(\frac{\partial V}{\partial T}\right)_P\right]^2\Big|_N = \frac{T}{NC_P^0}\left[\left(\frac{\partial \langle V\rangle_N}{\partial T}\right)_P\right]^2 \tag{24}$$

for the pure water system, where C_P^0 is heat capacity per water molecule (specific heat capacity), and

$$\frac{T}{C_P}\left[\left(\frac{\partial V}{\partial T}\right)_P\right]^2\Big|_{N,a} = \frac{T}{NC_P^0 + \Delta C_P}\left[\left(\frac{\partial[\langle V\rangle_N + \Delta V]}{\partial T}\right)_P\right]^2 \tag{25}$$

for the methane plus water system, where

$$C_P = NC_P^0 + \Delta C_P \tag{26}$$

and $\Delta C_P = -[\partial\{T^2\partial(\mu_a^*/T)/\partial T\}\partial T]_P$ is the excess heat capacity. [Theoretical ΔC_P values are obtained in our studies by using Eq. (19) to fit μ_a^*.] Physically, ΔC_P corresponds to the heat capacity of a box of N water molecules with a single methane at a fixed position minus the heat capacity of a box of N water molecules only (pure water) in the $N\to\infty$ limit. Similarly, the adiabatic excess compressibility

$$\mathcal{K}_S^o = \mathcal{K}_T^o - \left\{ \frac{T}{C_P}\left[\left(\frac{\partial V}{\partial T}\right)_P\right]^2\Big|_{N+a} - \frac{T}{C_P}\left[\left(\frac{\partial V}{\partial T}\right)_P\right]^2\Big|_N \right\}. \tag{27}$$

Here, the last term is identical to that in Eq. (24), whereas the first term enclosed by the curly brackets is now evaluated for a system with a methane that is free to move in water:

$$\frac{T}{C_P}\left[\left(\frac{\partial V}{\partial T}\right)_P\right]^2\Big|_{N+a} = \frac{T}{(C_P)_{N+a}}\left[\left(\frac{\partial \langle V\rangle_{N+a}}{\partial T}\right)_P\right]^2, \tag{28}$$

where $\langle V\rangle_{N+a} = \langle V\rangle_N + V_m$ [Eq. (4)]; and

$$(C_P)_{N+a} = NC_P^0 + \Delta C_P + \left[2k_BT\alpha^0 + k_BT^2\left(\frac{\partial\alpha^0}{\partial T}\right)_P + \frac{3k_B}{2}\right] \tag{29}$$

is equal to NC_P^0 plus terms (on the right hand side) for the partial molar heat capacity of methane, which consists of the excess heat capacity ΔC_P and contributions $k_B[\partial(T^2\partial \ln\langle V\rangle_N/\partial T)/\partial T]_P$ and $3k_B/2$ from, respectively, the translational degrees of freedom and kinetic energy of the

solute. The terms in square brackets in Eq. (29) follow because $\alpha^0=(\partial \ln\langle V\rangle_N/\partial T)_P$. Experimental expansitivity data[119] indicate that the terms in square brackets in Eq. (29) amount to ~ 20 J K^{-1} mol^{-1} (~ 5 cal K^{-1} mol^{-1}); and thus are small compared to the $\Delta C_P \sim 170-210$ J K^{-1} mol^{-1} ($\sim 40-50$ cal K^{-1} mol^{-1}) value obtained from experiment[95,125] and simulation.[63,67]

The relationship between partial molar adiabatic and isothermal compressibilities may also be derived by differentiating both sides of Eq. (22) with respect to the number, n, of methane solutes,

$$\mathcal{K}_S^o = \mathcal{K}_T^o - \frac{\partial}{\partial n}\left\{\frac{T}{C_P}\left[\left(\frac{\partial V}{\partial T}\right)_P\right]^2\right\}, \tag{30}$$

leading to[6,7]

$$\mathcal{K}_S^o = \mathcal{K}_T^o + T\left(\frac{\alpha^0}{\rho^0 C_P^0}\right)^2\left(\frac{\partial C_P}{\partial n}\right) - 2T\left(\frac{\alpha^0}{\rho^0 C_P^0}\right)\left(\frac{\partial V_m}{\partial T}\right)_P \tag{31}$$

in the infinite dilution limit [Eq. (31) is the $N\to\infty$ limit of Eq. (27)]. Here, from Eq. (29),

$$\frac{\partial C_P}{\partial n} = (C_P)_{N+a} - NC_P^0$$

$$= \Delta C_P + 2k_B T\alpha^0 + k_B T^2\left(\frac{\partial \alpha^0}{\partial T}\right)_P + \frac{3k_B}{2} \tag{32}$$

is the partial molar heat capacity of methane in water. Similarly, the $N\to\infty$ limit of Eq. (23) implies

$$\frac{\Delta\kappa_S}{\rho^0} = \frac{\Delta\kappa_T}{\rho^0} + T\Delta C_P\left(\frac{\alpha^0}{\rho^0 C_P^0}\right)^2 - 2T\left(\frac{\alpha^0}{\rho^0 C_P^0}\right)\left(\frac{\partial \Delta V}{\partial T}\right)_P, \tag{33}$$

which is equivalent to the relationship

$$\Delta\kappa_S = \Delta\kappa_T + \frac{T\alpha^0}{C_P^0}\left[\Delta C_P\left(\frac{\alpha^0}{\rho^0 C_P^0}\right) - 2\left(\frac{\partial V_m}{\partial T}\right)_P + 2k_B\kappa_T^0 + 2k_B T\left(\frac{\partial \kappa_T^0}{\partial T}\right)_P\right] \tag{34}$$

between the adiabatic and excess compressibilities in the infinite dilution limit.

Table I lists the experimental and theoretical TIP4P model quantities necessary to determine the adiabatic-isothermal difference in excess or partial molar compressibilities at $T=298$ K and $P=1$ atm from the above formulation. The computed theoretical values agree reasonably well with experimental measurements, with only two exceptions: The theoretical isothermal expansitivity of pure water, α^0, is about double that of the experimental value, as noted in Sec. III A; and the theoretical isobaric temperature derivative of isothermal compressibility of pure water, $(\partial\kappa_T^0/\partial T)_P$, is opposite in sign (albeit with a significantly smaller magnitude) to the corresponding experimental quantity.

Table I provides three estimates each for $\mathcal{K}_S^o-\mathcal{K}_T^o$ and $(\Delta\kappa_S-\Delta\kappa_T)/\rho^0$. One estimate is based solely on experimental data, whereas the other two estimates are theoretical and based on two different estimates of $(\partial\Delta V/\partial T)_P$ we obtained from Fig. 7. In every case, both excess and partial molar adiabatic compressibilities are smaller than their isothermal counterparts. Therefore, in view of our results above that the theoretical excess and partial molar isothermal compressibilities of methane in water are negative at 298 K and 1 atm, the inequality relations $\mathcal{K}_S^o<\mathcal{K}_T^o$ and $\Delta\kappa_S<\Delta\kappa_T$ in

TABLE I. Differences between adiabatic and isothermal partial molar and excess compressibilities of methane at 298.15 K under 1 atm are estimated using experimental and theoretical volumetric and thermodynamic data on pure water and aqueous solution of methane. Experimental data were taken from the published literature. Theoretical quantities were simulated using the TIP4P model of water; unless otherwise specified, they were determined in this work using the methods and formalism described in the text. The quantities tabulated along the experimental and theoretical columns were used exclusively to compute, respectively, the experimental and the theoretical compressibility differences $\mathcal{K}_S^o-\mathcal{K}_T^o$ and $(\Delta\kappa_S-\Delta\kappa_T)/\rho^0$ listed at the bottom rows of this table.

Volumetric and thermodynamic quantities	Unit	Expt.	Theor.
α^0	K^{-1}	(2.572×10^{-4})[a]	(5.64×10^{-4})[b]
ρ^0	mol cm^{-3}	0.0553[a]	0.0553[b]
κ_T^0	atm^{-1}	(4.588×10^{-5})[c]	(4.78×10^{-5})[d]
C_P^0	J mol^{-1} K^{-1}	75.3[e]	83.7[e]
$(\partial\alpha^0/\partial T)_P$	K^{-2}	(9.6×10^{-6})[f]	(8.8×10^{-6})[b]
$(\partial\kappa_T^0/\partial T)_P$	atm^{-1} K^{-1}	(-1.13×10^{-7})[f]	(2.5×10^{-8})[g]
$(\partial C_P/\partial n)$	J mol^{-1} K^{-1}	209.0[h]	193.5[i]
ΔC_P	J mol^{-1} K^{-1}	188.1[i]	171.7[j]
$(\partial V_m/\partial T)_P$	cm^3 mol^{-1} K^{-1}	0.270[k]	0.125[l] (0.029)[l]
$(\partial\Delta V/\partial T)_P$	cm^3 mol^{-1} K^{-1}	0.269[l]	0.120[m] (0.024)[n]
$\mathcal{K}_S^o-\mathcal{K}_T^o$	cm^3 mol^{-1} atm^{-1}	-9.84×10^{-4}	-7.85×10^{-4} (-0.77×10^{-4})[o]
$(\Delta\kappa_S-\Delta\kappa_T)/\rho^0$	cm^3 mol^{-1} atm^{-1}	-9.95×10^{-4}	-8.07×10^{-4} (-1.0×10^{-4})[o]

[a]From Table III of Kell (Ref. 119).
[b]From our simulation results in Fig. 2.
[c]Converted from the value provided in Table III of Kell (Ref. 119) in units of bar^{-1}.
[d]From *fitting* of the directly simulated volumes at four pressures in Figs. 8 and 9. The κ_T^0 value listed in this table is slightly different from the value of 5.13×10^{-5} atm^{-1} above, which was calculated using a different method that considered only the directly simulated data in Fig. 3 for 1 atm. Both of our theoretical κ_T^0 values are in reasonably good agreement with experiment.
[e]From Table 3 of Jorgensen and Madura, (Ref. 108), and references therein.
[f]Temperature derivatives at 25 °C were estimated using the data for 24°, 25°, and 26 °C in Table III of Kell (Ref. 119). The values for $(\partial\alpha^0/\partial T)_P$ and $(\partial\kappa_T^0/\partial T)_P$ are needed to convert between excess and partial molar quantities [Eqs. (29) and (34)].
[g]Estimated from the directly simulated volumes of pure water at $P=1$ atm, 1000 atm and $T=278$ K, 298 K in Fig. 2.
[h]From Table III of Naghibi *et al.* (Ref. 95).
[i]$(\partial C_P/\partial n)$ and ΔC_P are related by Eq. (32).
[j]From Fig. 2 of Moghaddam *et al.* (Ref. 67).
[k]Estimated from the methane partial molar volume data in Fig. 3 of Masterton (Ref. 93) (data included in Fig. 7 of the present paper).
[l]It follows from Eq. (9) that $(\partial V_m/\partial T)_P=(\partial\Delta V/\partial T)_P+k_B\kappa_T^0+k_BT(\partial\kappa_T^0/\partial T)_P$ [Eq. (34)].
[m]Estimated from the temperature dependence of ΔV from direct volume simulation (diamonds and dashed lines in Fig. 7).
[n]Estimated from the temperature dependence of ΔV as pressure derivative of simulated hydration free energy (circles and fitted dotted lines in Fig. 7).
[o]Theoretical $\mathcal{K}_S^o-\mathcal{K}_T^o$ and $(\Delta\kappa_S-\Delta\kappa_T)/\rho^0$ values shown without and with parentheses were calculated in accordance with Eqs. (31) and (33) using the theoretical $(\partial\Delta V/\partial T)_P$ value listed above which, respectively, is not (see footnote "m") and is (see footnote "n") enclosed in parentheses.

Table I imply that the excess and partial molar adiabatic compressibilities of methane in water are predicted by our model to be negative under the same conditions.

Amino acid partial molar adiabatic compressibilities have been determined experimentally to be negative at 298 K and 1 atm (e.g., $\mathcal{K}_S^o$ for glycine and lecine are,[84] respectively, -2.69×10^{-3} and -3.09×10^{-3} cm^3 mol^{-1} atm^{-1}). Based on these data and experimental $\mathcal{K}_S^o$ data for α, ω-aminocarboxylic acids,[1] the contribution of a methyl or methylene group in water to $\mathcal{K}_S^o$ at 25 °C under atmospheric pressure may be roughly estimated to be $\sim-1.0\times10^{-4}$ cm^3 mol^{-1} atm^{-1}. As far as the negative sign of the partial molar adiabatic compressibility is concerned, our model prediction of $\mathcal{K}_S^o<0$ and $\Delta\kappa_S<0$ for methane in water at 298 K and 1 atm is consistent with these experiments. However, quantitatively, the magnitude of our predicted negative $\mathcal{K}_S^o$ (an analogous discussion applies to $\Delta\kappa_S$) is at least one to two orders of magnitude larger than that of the above experimental estimate[1,84] of $\sim-1.0\times10^{-4}$ cm^3 mol^{-1} atm^{-1} for $\mathcal{K}_S^o$. For instance, using the isothermal $\mathcal{K}_T^o=-2.87\times10^{-4}$ cm^3 mol^{-1} atm^{-1} from the quadratic fits in Sec. III E and the experimental $\mathcal{K}_S^o-\mathcal{K}_T^o$ value in Table I, one arrives at $\mathcal{K}_S^o\approx-1.3\times10^{-3}$ cm^3 mol^{-1} atm^{-1}. If the lower theoretical estimate for $\mathcal{K}_S^o-\mathcal{K}_T^o$ in Table I is used, one obtains instead $\mathcal{K}_S^o\approx-3.6\times10^{-4}$ cm^3 mol^{-1} atm^{-1}; this value is of the same order of magnitude as the above experimental estimate of $\sim-1.0\times10^{-4}$ cm^3 mol^{-1} atm^{-1} for $\mathcal{K}_S^o$, but is more than three times larger in magnitude. If we used the $\mathcal{K}_T^o=-1.11\times10^{-3}$ cm^3 value computed above solely from the 1 atm volume distributions in Fig. 3, the negative signs of the theoretical and experimental $\mathcal{K}_S^o$'s again agree but their discrepancies in magnitude would be even larger.

We have documented in Table I the considerable numerical uncertainties in estimating $\mathcal{K}_S^o-\mathcal{K}_T^o$ and $(\Delta\kappa_S-\Delta\kappa_T)/\rho^0$. The values provided vary over approximately an order of magnitude. The main reason for the uncertainties is because the adiabatic-isothermal difference in excess or partial molar compressibility of methane is dependent upon the isobaric temperature derivative of its partial molar volume, $(\partial V_m/\partial T)_P$. But this quantity has not been studied extensively by experiments. Existing experimental and simulation data indicate that it is very sensitive to temperature (Fig. 7). Nonetheless, for the following reason, we believe that the inequality $\mathcal{K}_S^o<\mathcal{K}_T^o$ is likely a robust prediction for methane in water at 298 K and 1 atm. According to Eq. (31), $\mathcal{K}_S^o<\mathcal{K}_T^o$ is equivalent to the condition

$$\left(\frac{\partial V_m}{\partial T}\right)_P > \frac{\alpha^0}{2\rho^0 C_P^0}\left(\frac{\partial C_P}{\partial n}\right), \tag{35}$$

wherein the right hand side can be reliably determined to be 6.5×10^{-3} cm^3 mol^{-1} K^{-1} from the experimental data in Table I. It is noteworthy that this threshold $(\partial V_m/\partial T)_P$ value is significantly smaller than all of the experimental and theoretical estimates in Table I as well as the rough estimate of ~0.06 cm^3 mol^{-1} K^{-1} from the data of Kharakoz on aliphatic molecules[20] (see Sec. III D above). Hence, for methane in water at 298 K and 1 atm, $\mathcal{K}_S^o<\mathcal{K}_T^o$ most likely holds.

Obviously, when $\mathcal{K}_S^o<\mathcal{K}_T^o$, not only is $\mathcal{K}_S^o$ negative when $\mathcal{K}_T^o<0$, as is predicted by the present methane hydration model for 298 K and 1 atm, it is also possible, though not necessarily the case, for $\mathcal{K}_S^o$ to be negative when $\mathcal{K}_T^o>0$. Although we have studied only the adiabatic-isothermal difference in excess and partial molar compressibilities at 298 K and 1 atm, in future works the present method of analysis may be extended to other temperatures and pressures, including pressure regimes with $\mathcal{K}_T^o>0$ (upper panel of Fig. 9). Such an effort would be useful in addressing broader physical questions in the interpretation of volumetric and compressibility effects associated with conformational transitions of biomolecules.[16,17] In that regard, the temperature dependence of adiabatic-isothermic difference in partial molar compressibility would be of special interest in view of the possibility of sharp variation of $(\partial V_m/\partial T)_P$ with respect to T (Fig. 7).

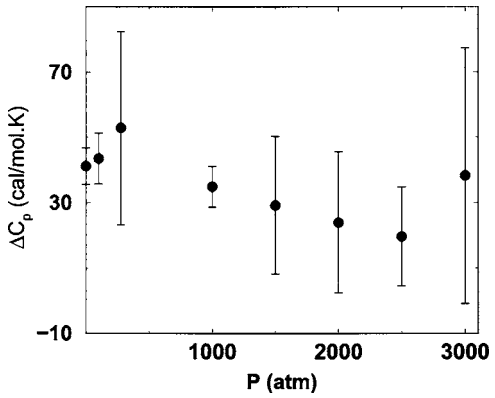

FIG. 10. Pressure dependence of model hydration heat capacity ΔG_P of methane, obtained by fitting Eq. (19) to the $\Delta G(P)$ values computed using test-particle insertion techniques at eight temperatures; $\Delta C_P=\Delta C_P(P)$ in Eq. (19). The error bars correspond to statistical uncertainties estimated by considering eight different heat capacity values obtained using seven (eight minus 1) ΔG values for the fit, with the ΔG value for a different T removed each time. The statistical uncertainty at pressure P is then taken to be plus or minus the range of variation among these eight different heat capacity values at the given P.

G. Pressure dependence of thermodynamic signatures

The temperature dependence of methane hydration at 1 atm has been studied computationally in considerable detail.[63,67] Here we examine the interplay between pressure and temperature effects. Figure 10 shows the hydration (excess) constant-pressure heat capacity of methane we computed using Eq. (19) at several pressures up to 3000 atm. There appears to be a slight decreasing trend for ΔC_P as pressure increases. But in view of the statistical uncertainties (error bars in the figure), we can only reasonably conclude that ΔC_P does not change significantly with pressure up to $P=3000$ atm, leaving a more precise determination of the model pressure dependence of ΔC_P to more extensive future simulations.

Experimental measurements show that the excess and partial molar heat capacity of methane in water (ΔC_P and $\partial C_P/\partial n$, respectively) decreases with increasing temperature at a moderate rate. The difference between ΔC_P and $\partial C_P/\partial n$ is small at 1 atm (see Sec. III F), and is expected to remain small at higher pressures.[126] At 1 atm, $\partial C_P/\partial n$ of methane in water has been measured by Rettich *et al.*[94] for several tem-

peratures ranging from $T=273.15$ to 333.15 K, with $\partial C_P/\partial n$ values ranging from 262 J mol^{-1} K^{-1} at 273.15 K to 201 J mol^{-1} K^{-1} at 313.15 K; hence $[\partial(\partial C_P/\partial n)/\partial T]_P \approx -1.0$ J mol^{-1} K^{-2}. Subsequently, also at 1 atm, Naghibi *et al.*[95] measured $\partial C_P/\partial n$ for the temperature range between $T=273.15$ and 323.15 K, yielding a maximum $\partial C_P/\partial n=226.9$ J mol^{-1} K^{-1} at 273.15 K and a minimum $\partial C_P/\partial n=191.0$ J mol^{-1} K^{-1} at 323.15 K, with $[\partial(\partial C_P/\partial n)/\partial T]_P \approx -0.72$ J mol^{-1} K^{-2}.

The ΔC_P values we computed are assumed to be temperature independent [Eq. (19)]. At 1 atm, our previously determined[63,67] $\Delta C_P=171.7$ J mol^{-1} K^{-1} (41.07 cal mol^{-1} K^{-1}), which correspond to $\partial C_P/\partial n=193.5$ J mol^{-1} K^{-1} (46.3 cal mol^{-1} K^{-1}), is in reasonably good agreement with the experimentally determined values in the aforementioned temperature ranges. We have attempted to estimate the temperature dependence of ΔC_P from our computational results. But the simulated free energies we obtained from particle insertions apparently did not possess the very high precision necessary for meaningfully extracting a third temperature derivative.

Pressure effects on hydration heat capacities of several solutes were addressed experimentally by Hnědkovský and Wood,[96] who have determined the hydration heat capacity of methane under a pressure of 28.0 MPa (276.3 atm) at two temperatures. They found that $\partial C_P/\partial n=244.7$ J mol^{-1} K^{-1} at 303.96 K and $\partial C_P/\partial n=210.0$ J mol^{-1} K^{-1} at 373.58 K. Interestingly, their results suggest that under this elevated pressure, $[\partial(\partial C_P/\partial n)/\partial T]_P \approx -0.5$ J mol^{-1} K^{-2}, which is a lower rate of decrease with respect to temperature relative to that under atmospheric pressure. Moreover, these experimental data also suggest that for the range of temperatures between 273.15 and 373.15 K, $\partial C_P/\partial n$ values at 276.3 atm are on average 10%–20% higher than that at 1 atm. If we extrapolate the available experimental data to cover the entire temperature range from 273.15 to 373.15 K, the 1 atm data of Rettich *et al.*[94] and Naghibi *et al.*[95] yield average $\partial C_P/\partial n$ values of 212.0 and 190.9 J mol^{-1} K^{-1}, respectively. In comparison, the 276.3 atm data of Hnědkovský and Wood[96] yield a corresponding average $\partial C_P/\partial n$ of 235.2 J mol^{-1} K^{-1}. For $P=276.3$ atm, our present simulation results give $\Delta C_P=221.0$ J mol^{-1} K^{-1} (52.9 cal mol^{-1} K^{-1}; see Fig. 10), which is ≈29% higher than the ΔC_P value we computed for 1 atm. Although more extensive computation will be needed to ascertain whether this increase in the computed value of ΔC_P from 1 to 276.3 atm is statistically significant, the general trend observed in our simulation results in Fig. 10 indicating no big variation of ΔC_P when pressure in increased above $P=1$ atm is consistent with the experiment of Hnědkovský and Wood[96] as the difference $\partial C_P/\partial n-\Delta C_P$ is expected to depend only weakly on P within this pressure range.[126]

Figure 11 shows the enthalpic and entropic components of our model methane hydration free energy at 298 K as functions of pressure. There is a clear trend of increasing enthalpic unfavorability: ΔH_0 changes from being favorable (<0) at low pressures to being unfavorable (>0) at high pressures, with a crossover point around $P\sim 1500$ atm. In contrast, the entropic free energy $-T_0\Delta S_0$ exhibits neither a systematic increasing nor decreasing trend. Taken together,

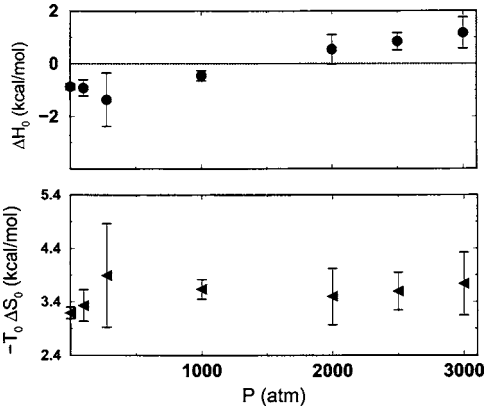

FIG. 11. Pressure dependence of model methane hydration enthalpy ΔH_0 (upper panel) and entropic component $-T_0\Delta S_0$ of free energy at $T_0=298$ K, obtained by fitting Eq. (19) to the $\Delta G(P)$ values from test-particle insertions; ΔH_0 and ΔS_0 are equal to, respectively, $\Delta H_0(P)$ and $\Delta S_0(P)$ in Eq. (19). Statistical uncertainties (error bars) are estimated for the fitted enthalpy and entropy as for the fitted heat capacity in Fig. 10.

these findings imply that the trend of increasing unfavorability of methane hydration with pressure (ΔG increases with P, see Fig. 4) is driven mainly by enthalpy.

Because the only source of entropy in our model system is from the water molecules, the results in Fig. 11 suggest that within the range of pressures studied, water-water hydrogen bonds around a small nonpolar solute are essentially maintained at room temperature irrespective of pressure. Thus the increased enthalpic unfavorability of hydration of the small nonpolar solute at elevated pressure is likely a result of increased van der Waals repulsion between the solute and the water molecules. This trend may be consistent with x-ray absorption data suggesting little pressure effect (up to ~700 atm) on the water structure in the vicinity of a solvated krypton.[46] These structural and energetic issues deserve further exploration in future works.

IV. CONCLUDING REMARKS

Using a combination of test-particle insertion and direct volume simulation techniques, we have examined the thermodynamic and volumetric behaviors of hydrophobic hydration of a methanelike solute, paying special attention to heat capacity and compressibility, quantities that are second derivatives of free energy. For properties that have been measured experimentally, we found good agreements between our computational results and experimental data. These include the isothermal compressibility, its temperature derivative, and the temperature derivative of isobaric thermal expansitivity of pure water under atmospheric pressure, as well as the partial molar heat capacity of methane, its partial molar volume, and the temperature variation of the partial molar volume, among other properties. In particular, our computational results indicate that hydration heat capacity of a methanelike solute is not considerably pressure sensitive, a trend that is consistent with previous experimental measurements conducted under pressures up to ~280 atm.

The match between theory and experiment is not perfect. Nonetheless, the good agreement between the two as observed here suggests that a combination of van der Waals

interactions and a simple accounting of water-water hydrogen bonding, features that are embodied in the TIP4P model, may be sufficient to capture much of the essential physics governing the temperature and pressure dependence of hydrophobic hydration. Also, the good agreement between theory and existing experiment lends credence—even if it is only tentative—to model predictions in temperature and pressure regimes for which experimental data are not yet available.

At 1 atm, our simulation results are consistent with a negative partial molar isothermal compressibility and an even more negative partial molar adiabatic compressibility for a methanelike nonpolar group in water. The latter prediction is consistent with experiments. However, there are considerable computational and experimental uncertainties in estimating the adiabatic-isothermal difference in partial molar compressibility that remains to be addressed.

At pressure >1000 atm, results from our direct volume simulations reveal a robust trend of increasingly positive partial molar isothermal compressibility of methane in water under high pressures. If aqueous solvation of methane is taken as a mimicry of generic exposure of nonpolar groups to water, the partial molar isothermal compressibility trend predicted by our model is consistent with and, thus, contributes to a rationalization for the experimental observations that pressure-induced unfolding transitions of proteins are predominantly accompanied by positive changes in isothermal compressibility. Remarkably, the pressure dependence of our computed partial molar isothermal compressibility of methane, which covers a range of 3000 atm, echoes that of experimental partial molar adiabatic compressibilities of nonpolar groups deduced from model compound measurements. Although further analysis is needed to better connect the two sets of data, this apparent match between theory and experiment is particularly encouraging to the endeavor of putting adiabatic compressibility measurement as a probe of conformational transitions[1,7,16,17,20,84] on a more definitive physical basis.

Clearly, in spite of what we have learned, our current knowledge on the issues raised above is very limited. Much remains to be discovered. Results from the present study and the methodology developed here set the stage for more extensive investigations of the interplay of pressure and temperature effects in nonpolar hydration and hydrophobic interactions in more complex situations. In this regard, it would be particularly instructive, for example, to evaluate the robustness of the present observations by comparing them with predictions from other models of water,[66,127–130] as has been insightfully performed in a detailed analysis[66] of the separation-dependent heat capacity of hydrophobic interactions.[64]

ACKNOWLEDGMENTS

The authors thank Dr. Tigran Chalikian, Dr. Zhirong Liu, Dr. Seishi Shimizu, Dr. Nicolas Taulier, and Dr. Roland Winter for helpful discussions. The research reported here was supported by the Canadian Institutes of Health Research (CIHR Grant no. MOP-15323). One of the authors (M.S.M.) was supported in part by a Premier's Research Excellence Award from the Province of Ontario to the other author (H.S.C.) who holds a Canada Research Chair in Proteomics, Bioinformatics and Functional Genomics.

[1] T. V. Chalikian, A. P. Sarvazyan, and K. J. Breslauer, Biophys. Chem. **51**, 89 (1994).
[2] T. V. Chalikian and K. J. Breslauer, Biopolymers **39**, 619 (1996).
[3] P. W. Bridgman, J. Biol. Chem. **19**, 511 (1914).
[4] G. Panick, G. J. A. Vidugiris, R. Malessa, G. Rapp, R. Winter, and C. A. Royer, Biochemistry **38**, 4157 (1999).
[5] W. Dzwolak, R. Ravindra, J. Lendermann, and R. Winter, Biochemistry **42**, 11347 (2003).
[6] M. J. Blandamer, M. I. Davis, F. Douhéret, and J. C. R. Reis, Chem. Soc. Rev. **30**, 8 (2001).
[7] N. Taulier and T. V. Chalikian, Biochim. Biophys. Acta **1595**, 48 (2002).
[8] K. Gekko, Biochim. Biophys. Acta **1595**, 382 (2002).
[9] I. Bezsonova, D. M. Korzhnev, R. S. Prosser, J. D. Forman-Kay, and L. E. Kay, Biochemistry **45**, 4711 (2006).
[10] D. M. Korzhnev, I. Bezsonova, F. Evanics, N. Taulier, Z. Zhou, Y. Bai, T. V. Chalikian, R. S. Prosser, and L. E. Kay, J. Am. Chem. Soc. **128**, 5262 (2006).
[11] H. Seeman, R. Winter, and C. A. Royer, J. Mol. Biol. **307**, 1091 (2001).
[12] C. Dirix, F. Meersman, C. E. MacPhee, C. M. Dobson, and K. Heremans, J. Mol. Biol. **347**, 903 (2005).
[13] F. Meersman and C. M. Dobson, Biochim. Biophys. Acta **1764**, 452 (2006).
[14] R. Ravindra, S. Zhao, H. Gies, and R. Winter, J. Am. Chem. Soc. **126**, 12224 (2004).
[15] J. D. Batchelor, A. Olteanu, A. Tripathy, and G. J. Pielak, J. Am. Chem. Soc. **126**, 1958 (2004).
[16] T. V. Chalikian, Annu. Rev. Biophys. Biomol. Struct. **32**, 207 (2003).
[17] R. Ravindra and R. Winter, ChemPhysChem **4**, 359 (2003).
[18] S. Shimizu, Proc. Natl. Acad. Sci. U.S.A. **101**, 1195 (2004).
[19] P. E. Smith, Biophys. Chem. **113**, 299 (2005).
[20] D. P. Kharakoz, Biophys. Chem. **34**, 115 (1989).
[21] D. P. Kharakoz, J. Phys. Chem. **95**, 5634 (1991).
[22] P. Gianni and L. Lepori, J. Solution Chem. **25**, 1 (1996).
[23] W. Kauzmann, Adv. Protein Chem. **14**, 1 (1959).
[24] J. F. Brandts, in *Structure and Stability of Biological Macromolecules*, edited by S. N. Timasheff and G. D. Fasman (Dekker, New York, 1969), p. 213.
[25] C. Tanford, *The Hydrophobic Effect: Formation of Micelles and Biological Membranes* (Wiley, New York, 1980).
[26] A. Ben-Naim, *Hydrophobic Interactions* (Plenum, Oxford, 1980).
[27] K. A. Dill, Biochemistry **29**, 7133 (1990).
[28] W. Blokzijl and J. B. F. N. Engberts, Angew. Chem., Int. Ed. Engl. **32**, 1545 (1993).
[29] H. S. Chan and K. A. Dill, Annu. Rev. Biophys. Biomol. Struct. **26**, 425 (1997).
[30] H. A. Scheraga, J. Biomol. Struct. Dyn. **16**, 447 (1998).
[31] J. M. Sorenson, G. Hura, A. K. Soper, A. Pertsemlidis, and T. Head-Gordon, J. Phys. Chem. B **103**, 5413 (1999).
[32] G. Hummer, S. Garde, A. E. García, and L. E. Pratt, Chem. Phys. **258**, 349 (2000).
[33] N. T. Southall, K. A. Dill, and A. D. J. Haymet, J. Phys. Chem. B **106**, 521 (2002); Correction: **106**, 2812 (2002).
[34] L. R. Pratt, Annu. Rev. Phys. Chem. **53**, 409 (2002).
[35] B. Widom, P. Bhimalapuram, and K. Koga, Phys. Chem. Chem. Phys. **5**, 3085 (2003).
[36] K. A. Dill, T. M. Truskett, V. Vlachy, and B. Hribar-Lee, Annu. Rev. Biophys. Biomol. Struct. **34**, 173 (2005).
[37] T. M. Raschke and M. Levitt, Proc. Natl. Acad. Sci. U.S.A. **102**, 6777 (2005).
[38] C. N. Pace, Biochemistry **40**, 310 (2001).
[39] T. V. Chalikian, Biopolymers **70**, 492 (2003).
[40] M. Auton and D. W. Bolen, Proc. Natl. Acad. Sci. U.S.A. **102**, 15065 (2005).
[41] A. Wallqvist, J. Chem. Phys. **96**, 1655 (1992).
[42] N. Matubayasi and R. M. Levy, J. Phys. Chem. **100**, 2681 (1996).
[43] P.-L. Chau and R. L. Mancera, Mol. Phys. **96**, 109 (1999).
[44] R. D. Broadbent and G. W. Neilson, J. Chem. Phys. **100**, 7543 (1994).
[45] P. H. K. De Jong, J. E. Wilson, G. W. Neilson, and A. D. Buckingham,

Mol. Phys. **91**, 99 (1997).
[46] D. T. Bowron, R. Weigel, A. Filipponi, M. A. Roberts, and J. L. Finney, Mol. Phys. **99**, 761 (2001).
[47] A. D. Robertson and K. P. Murphy, Chem. Rev. (Washington, D.C.) **97**, 1251 (1997).
[48] H. S. Chan and K. A. Dill, J. Chem. Phys. **101**, 7007 (1994).
[49] R. H. Wood and P. T. Thompson, Proc. Natl. Acad. Sci. U.S.A. **87**, 8921 (1990).
[50] V. Martorana, D. Bulone, P. L. San Biagio, M. B. Palma-Vittorelli, and M. U. Palma, Biophys. J. **73**, 31 (1997).
[51] S. Shimizu and H. S. Chan, J. Chem. Phys. **115**, 1414 (2001).
[52] H. S. Chan, S. Shimizu, and H. Kaya, Methods Enzymol. **380**, 350 (2004).
[53] K. Lum, D. Chandler, and J. D. Weeks, J. Phys. Chem. B **103**, 4570 (1999).
[54] P. R. ten Wolde, J. Phys.: Condens. Matter **14**, 9445 (2002).
[55] S. Singh, J. Houston, F. van Swol, and C. J. Brinker, Nature (London) **442**, 526 (2006).
[56] S. Shimizu and H. S. Chan, Proteins **48**, 15 (2002); **49**, 294(E) (2002).
[57] Y. Levy and J. N. Onuchic, Annu. Rev. Biophys. Biomol. Struct. **35**, 389 (2006).
[58] Z. Liu and H. S. Chan, J. Mol. Biol. **349**, 872 (2005).
[59] D. A. d'Avignon, G. L. Bretthorst, M. E. Holtzer, K. A. Schwarz, R. H. Angeletti, L. Mints, and A. Holtzer, Biopolymers **83**, 255 (2006).
[60] J. L. MacCallum, M. S. Moghaddam, H. S. Chan, and D. P. Tieleman, Proc. Natl. Acad. Sci., U.S.A. (in press).
[61] D. Rodriguez-Larrea, S. Minning, T. V. Borchert, and J. M. Sanchez-Ruiz, J. Mol. Biol. **360**, 715 (2006).
[62] Z. Liu and H. S. Chan, Phys. Biol. **2**, S75 (2005).
[63] S. Shimizu and H. S. Chan, J. Chem. Phys. **113**, 4683 (2000); **116**, 8636(E) (2002).
[64] S. Shimizu and H. S. Chan, J. Am. Chem. Soc. **123**, 2083 (2001).
[65] S. W. Rick, J. Phys. Chem. B **107**, 9853 (2003).
[66] D. Paschek, J. Chem. Phys. **120**, 6674 (2004).
[67] M. S. Moghaddam, S. Shimizu, and H. S. Chan, J. Am. Chem. Soc. **127**, 303 (2005); **127**, 2363(E) (2005).
[68] D. Paschek, J. Chem. Phys. **120**, 10605 (2004).
[69] G. Graziano, J. Chem. Phys. **123**, 034509 (2005).
[70] S. Shimizu and H. S. Chan, Proteins **49**, 560 (2002).
[71] W. Kauzmann, Nature (London) **325**, 763 (1987).
[72] G. Hummer, S. Garde, A. E. García, A. Pohorille, and L. R. Pratt, Proc. Natl. Acad. Sci. U.S.A. **93**, 8951 (1996).
[73] G. Hummer, S. Garde, A. E. García, M. E. Paulaitis, and L. R. Pratt, Proc. Natl. Acad. Sci. U.S.A. **95**, 1552 (1998).
[74] V. M. Dadarlat and C. B. Post, J. Phys. Chem. B **105**, 715 (2001).
[75] V. A. Payne, N. Matubayasi, L. R. Murphy, and R. M. Levy, J. Phys. Chem. B **101**, 2054 (1997).
[76] T. Ghosh, A. E. García, and S. Garde, J. Chem. Phys. **116**, 2480 (2002).
[77] T. Ghosh, A. E. García, and S. Garde, J. Phys. Chem. B **107**, 612 (2003).
[78] D. Paschek and A. E. García, Phys. Rev. Lett. **93**, 238105 (2004).
[79] D. Paschek, S. Gnanakaran, and A. E. García, Proc. Natl. Acad. Sci. U.S.A. **102**, 6765 (2005).
[80] D. Paschek, S. Nonn, and A. Geiger, Phys. Chem. Chem. Phys. **7**, 2780 (2005).
[81] V. Dadarlat and C. B. Post, Proc. Natl. Acad. Sci. U.S.A. **100**, 14778 (2003).
[82] V. Dadarlat and C. B. Post, Biophys. J. **91**, 4544 (2006).
[83] K. Mori, Y. Seki, Y. Yamada, H. Matsumoto, and K. Soda, J. Chem. Phys. **125**, 054903 (2006).
[84] A. P. Sarvazyan and T. V. Chalikian, in *Ultrasonics International 89 Conference Proceedings* (Butterworth, Madrid, Spain, 1989), p. 704.
[85] D. M. Lockwood and P. J. Rossky, J. Phys. Chem. B **103**, 1982 (1999).
[86] D. M. Lockwood, P. J. Rossky, and R. M. Levy, J. Phys. Chem. B **104**, 4210 (2000).
[87] Y. Harano, T. Imai, A. Kovalenko, M. Kinoshita, and F. Hirata, J. Chem. Phys. **114**, 9506 (2001).
[88] T. Imai and F. Hirata, J. Chem. Phys. **122**, 094509 (2005).
[89] M. I. Marqués, J. M. Borreguero, H. E. Stanley, and N. V. Dokholyan, Phys. Rev. Lett. **91**, 138103 (2003).
[90] K. Koga, J. Chem. Phys. **121**, 7304 (2004).
[91] J. K. Cheung, P. Shah, and T. M. Truskett, Biophys. J. **91**, 2427 (2006).
[92] S. W. Rick, J. Phys. Chem. B **104**, 6884 (2000).
[93] W. L. Masterton, J. Chem. Phys. **22**, 1830 (1954).
[94] T. R. Rettich, Y. P. Handa, R. Battino, and E. Wilhelm, J. Phys. Chem. **85**, 3230 (1981).
[95] H. Naghibi, S. F. Dec, and S. J. Gill, J. Phys. Chem. **90**, 4621 (1986).
[96] L. Hnědkovský and R. H. Wood, Thermodyn. **29**, 731 (1997).
[97] K. Hata, R. Kono, M. Fujisawa, R. Kitahara, Y. O. Kamatari, K. Akaska, and Y. Xu, Cell Mol. Biol. (Paris) **50**, 311 (2004).
[98] E. Ohmae, K. Kubota, K. Nakasone, C. Kato, and K. Gekko, Chem. Lett. **33**, 798 (2004).
[99] G. I. Makhatadze and P. L. Privalov, J. Mol. Biol. **213**, 375 (1990).
[100] P. L. Privalov and G. I. Makhatadze, J. Mol. Biol. **213**, 385 (1990).
[101] H. Kaya and H. S. Chan, Proteins **40**, 637 (2000); **43**, 523(E) (2001).
[102] A. I. Dragan and P. L. Privalov, J. Mol. Biol. **321**, 891 (2002).
[103] M. Knott and H. S. Chan, Proteins **65**, 373 (2006).
[104] S. Cao and S.-J. Chen, RNA-A Publication of the RNA Soc. **11**, 1884 (2005).
[105] A. Tikhomirova, I. V. Beletskaya, and T. V. Chalikian, Biochemistry **45**, 10563 (2006).
[106] A. N. Naganathan, R. Perez-Jimenez, J. M. Sanchez-Ruiz, and V. Muñoz, Biochemistry **44**, 7435 (2005).
[107] W. L. Jorgensen, J. Chandrasekhar, J. D. Madura, R. W. Impey, and M. L. Klein, J. Chem. Phys. **79**, 926 (1983).
[108] W. L. Jorgensen and J. D. Madura, Mol. Phys. **56**, 1381 (1985).
[109] W. L. Jorgensen, BOSS Version 4.1, Yale University, New Haven, CT, 1999.
[110] A. Ben-Naim, *Solvation Thermodynamics* (Plenum, New York, 1987), pp. 127–132.
[111] S. Shimizu, M. S. Moghaddam, and H. S. Chan, J. Phys. Chem. B **109**, 21220 (2005).
[112] C. Czaplewski, S. Kalinowski, A. Liwo, D. R. Ripoll, and H. A. Scheraga, J. Phys. Chem. B **109**, 21222 (2005).
[113] C. Czaplewski, S. Kalinowski, A. Liwo, and H. A. Scheraga, Mol. Phys. **103**, 3153 (2005).
[114] Same as the type of ensembles used in particle-insertion computation of two-methane potentials of mean force; e.g., in Ref. 63.
[115] W. L. Jorgensen, Chem. Phys. Lett. **92**, 405 (1982).
[116] M. F. Floris, J. Phys. Chem. B **108**, 16244 (2004).
[117] R. K. Pathria, *Statistical Mechanics* (Pergamon, Oxford, UK, 1980), p. 109.
[118] NIST Chemistry WebBook, NIST Standard Reference Database Number 69, edited by P. J. Linstrom and W. G. Mallard (National Institute of Standards and Technology, Gaithersburg, MD, 2005); http://webbook.nist.gov
[119] G. S. Kell, J. Chem. Eng. Data **20**, 97 (1975).
[120] K. A. Dill, D. O. V. Alonso, and K. Hutchinson, Biochemistry **28**, 5439 (1989).
[121] D. O. V. Alonso and K. A. Dill, Biochemistry **30**, 5974 (1991).
[122] K. A. Dill and S. Stigter, Adv. Protein Chem. **46**, 59 (1995).
[123] Indeed, the high value of the predicted methane excess compressibility in Ref. 42 led to the puzzling result that a hypothetical solution of one molar methane in water (i.e., the mole fraction of methane is only ~0.018) could more than double the compressibility relative to that of pure water [i.e., increase κ_T by $(5.8\pm4.7)\times10^{-5}$ atm^{-1} to $(10.8\pm4.8)\times10^{-5}$ atm^{-1} from the compressibility $\kappa_T^0\sim5.0\times10^{-5}$ atm^{-1} for pure water; see page 2684 of Ref. 42].
[124] The analysis in the lower panel of Fig. 9 assumed group additivity and neglected a possible difference in contribution to partial molar compressibility from methyl and methylene groups (see, e.g., discussion in Ref. 86).
[125] T. J. Morrison and F. Billett, J. Chem. Soc. 3819 (1952).
[126] This is because the α^0 and $(\partial\alpha^0/\partial T)_P$ factors that determine the difference $(\partial C_P/\partial n-\Delta C_P)$ in Eq. (32) do not appear to increase with increasing P, as is evident from the lower panel in Fig. 2, which shows a very gradual decrease in both the slope and curvature of the $\langle V\rangle_N$ vs T curves as pressure increases.
[127] D. van Belle and S. J. Wodak, J. Am. Chem. Soc. **115**, 647 (1993).
[128] S. W. Rick, S. J. Stuart, and B. J. Berne, J. Chem. Phys. **101**, 6141 (1994).
[129] W. S. Young and C. L. Brooks III, J. Chem. Phys. **106**, 9265 (1997).
[130] W. L. Jorgensen and J. Tirado-Rives, Proc. Natl. Acad. Sci. U.S.A. **102**, 6665 (2005).